6-1991

Resonant Electron Transfer and K-Shell Excitation of F^{q+} (Q=6,8) in Collisions with Neutral He and H^2 Targets

Konstantinos E. Zaharakis
Western Michigan University

RESONANT ELECTRON TRANSFER AND K-SHELL EXCITATION OF F^{q+} (q=6,8) IN COLLISIONS WITH NEUTRAL He AND H_2 TARGETS

by

Konstantinos E. Zaharakis

A Thesis
Submitted to the
Faculty of The Graduate College
in partial fulfillment of the
requirements for the
Degree of Master of Arts
Department of Physics

Western Michigan University
Kalamazoo, Michigan
June 1991

RESONANT ELECTRON TRANSFER AND K-SHELL EXCITATION OF F^{q+} (q=6,8) IN COLLISIONS WITH NEUTRAL He AND H_2 TARGETS

Konstantinos E. Zaharakis, M.A.

Western Michigan University, 1991

Measurements of resonant transfer and excitation (RTE) were conducted for 16.5-38 MeV F^{6+} (Li-like) ions colliding with H_2. In the RTE process electron capture and projectile excitation take place simultaneously due to the electron-electron interaction. In previous work, for the same collision system, at the Oak Ridge National Laboratory (Oak Ridge, TN), the magnitude of the measured RTE cross sections was found to be nearly a factor of two smaller than theory. In order to investigate RTE in F^{6+} + H_2 collisions more completely, we undertook measurements at Western Michigan University using the EN tandem Van de Graaff accelerator, and, additionally, related measurements were made for F^{q+} + H_2 and F^{q+} + He collision systems with q=8 and 9. The present RTE cross sections for F^{6+} + H_2 are about 70% larger than those obtained at Oak Ridge and show good agreement with theoretical predictions.

Εἰς μνὴμην τοῦ πατρὸς μου

Ἠλὶα Ζαχαρὰκη

I dedicate this Thesis in memory

of my father Elias Zaharakis

ACKNOWLEDGEMENTS

I would like to acknowledge my indebtedness to the people who have in various ways contributed to this study.

First of all, I wish to thank my research advisors, Dr. John A. Tanis and Dr. Eugene M. Bernstein, for their patient guidance and instruction and for their constructive criticism. Without their help this project could never have been completed. I also wish to thank Dr. Steven M. Ferguson for operating the Western Michigan University Van de Graaff Accelerator and Dr. Mark W. Clark for assisting me during the early stages of this work.

Thanks are also due to the remaining members of the faculty of the Department of Physics for their sincere interest and encouragement during my time as a student at Western Michigan University, Kalamazoo.

Finally, I want to express my gratitude to my family who have supported me during all these years that I have been away from home. It is their support that has given me strength to be able to overcome all the difficulties that I have experienced.

Konstantinos E. Zaharakis

Order Number 1345224

Resonant electron transfer and K-shell excitation of F^{q+} (q = 6,8) in collisions with neutral He and H_2 targets

Zaharakis, Konstantinos Elias, M.A.

Western Michigan University, 1991

U·M·I
300 N. Zeeb Rd.
Ann Arbor, MI 48106

TABLE OF CONTENTS

LIST OF TABLES

LIST OF FIGURES

List of Figures - continued

CHAPTER I

INTRODUCTION

A basic problem in atomic physics is to study collisions of particles, and specifically collisions of projectile ions with neutral target atoms. There are three major categories of events that occur in an ion-atom collision (Hasted, 1972).

1. Excitation: Electrons are excited from lower to higher energy states within the ion and, as a result, vacancies are produced in the energy levels originally occupied by the excited electrons.

2. Ionization: Loss of one or more electrons by the ion or atom.

3. Charge transfer: Electrons from the neutral target are captured by the projectile ion (the target atom is ionized).

All three processes can be attributed to the Coulomb force between the interacting particles and therefore they are related. Each process takes place due to the direct interaction between the nucleus of one colliding partner and the electrons of the other or between electrons of the projectile ions and electrons of the target atoms. The

distance between the interacting particles, their charge, and the energy at which the collision takes place are the three basic factors that govern excitation, ionization and charge transfer. These processes can occur in either collision partner or in both, and it is important to note that combinations of these processes can occur as well.

Let us consider an ion-atom collision in which the ion serves as a projectile and the atom as a target. We want to focus on the combined process of electron capture by the ion and excitation of this same collision partner. While any excitation is possible we will consider only those that give rise to K-shell vacancies, i.e., an electron is promoted from $n = 1$ to $n \geq 2$. The captured electron may occupy any unoccupied bound state of the ion. This charge-changed excited state of the ion will subsequently decay by emitting either a photon (x ray) or an electron (Auger emission). These events which result in capture and K-shell excitation, yielding an intermediate doubly-excited state, and which subsequently decay by x-ray emission, are the primary emphasis of this thesis.

There are three basic mechanisms by which this combined electron transfer and ion excitation can proceed. One is a two-step process called non resonant transfer and excitation (NTE) (Pepmiller, 1983; 1985), in which the projectile is first excited through the Coulomb interaction

with the target nucleus and subsequently captures an electron from the target (a target electron-projectile nucleus interaction). It should be noted that the excitation and capture events are independent.

If the combined process is due to the electron-electron interaction between an electron of the projectile and a (weakly bound) target electron, resonant formation of intermediate states can occur for specific incident ion velocities (i.e., velocities that correspond to Auger electron velocities; see Chapter II). In this process transfer and excitation take place simultaneously (i.e., it is a correlated process) and is called resonant transfer and excitation (RTE) with x-ray emission (Tanis et al., 1981).

The third mechanism by which this combined electron transfer and ion excitation can proceed is called two electron transfer and excitation (2eTE) (Hahn, 1985; Schulz et al., 1988; Hahn and Ramadan, 1989) which is an uncorrelated process as in the case of NTE. Again, in this process, a target electron is captured by the projectile and a projectile electron is excited. Here, however, the excitation is not due to an interaction with the captured electron as in RTE, or with the target nucleus, as in NTE, but with a second target electron. Therefore, in 2eTE excitation and capture are not correlated and no resonant

behavior is expected.

RTE is analogous to the fundamental ion-electron recombination process referred to as dielectronic recombination (DR) (Seaton and Storey, 1976). The only difference between RTE and DR is that in RTE the captured electron is initially bound in an atom while in DR the captured electron is free.

Both processes can lead to the same intermediate excited states. DR is a process which is responsible for energy dissipation in fusion plasmas. Since energy production from fusion plasmas is of great importance, DR is a mechanism that has been studied extensively. Laboratory measurements of DR are in general difficult to obtain while RTE experiments are relatively easy to perform. Since 1981 when it was first proposed (Tanis et al., 1981), RTE has become the subject of many experimental and theoretical studies, and today the close relationship between RTE and DR is clearly established. Therefore, the study of RTE provides a means of studying DR and that makes RTE a process of considerable interest.

The main purpose of this thesis is to present new experimental work that has been done to investigate RTE for the $F^{6+} + H_2$ system. Previous measurements for this collision system made at the Oak Ridge National Laboratory, Oak Ridge, TN, show a discrepancy of a factor of two

between theory and experiment. In addition, related measurements were made for F^{q+} + H_2 collisions and for F^{q+} + He collision systems with q = 6,8,9.

CHAPTER II

THEORETICAL CONSIDERATIONS

In the collision between an ion and an atom, projectile ion excitation and electron capture from the target atom can occur together, in a single encounter, resulting in the formation of an intermediate doubly excited state. This intermediate excited state decays by either photon (x-ray) emission or electron (Auger) emission.

In general, these reactions are expressed by the notation:

$$A^{q+} + B \rightarrow [A^{(q-1)+}]^{**} + B^{+} \begin{cases} \rightarrow A^{(q-1)+} + h\nu \\ \rightarrow A^{q+} + e^{-} \end{cases} \qquad (2.1)$$

For a Li-like (i.e., three-electron) ion, these reactions are shown schematically in Figure 1.

It is noted that electron emission occurs in the de-excitation of the intermediate state when one electron falls to the K-shell without emission of radiation. The ejected electron is called an Auger electron and its kinetic energy (K) depends upon its binding energy E_n before emission and upon the energy difference between the excited and ground states of the ion, ΔE, i.e., $K = \Delta E - E_n$. It

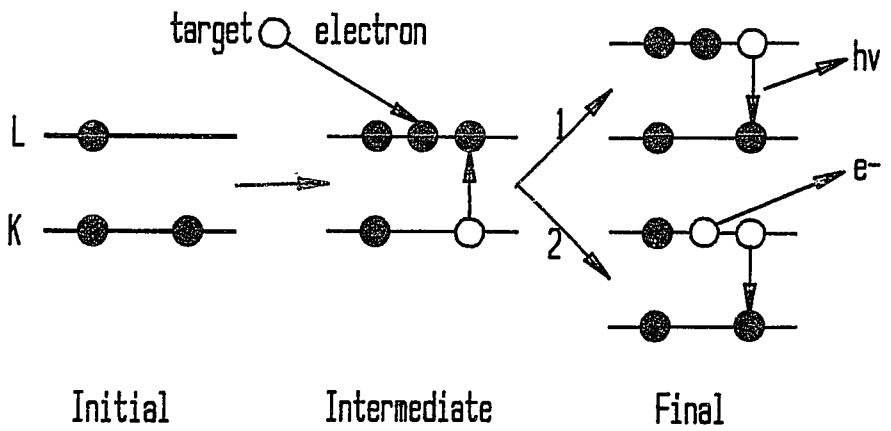

Figure 1. Schematic Indicating the Initial, Intermediate, and Final States of a Li-Like Ion Undergoing Combined Capture and Excitation When Colliding With a Target Atom.

should be noted that ΔE is the difference in energy between the initial and final states which are in two different ions since the charge state increases with Auger emission. Since electrons that are bound in an ion obey quantization rules, ΔE and E_n have discrete values so K has discrete values also. Therefore, the energy of the Auger electron is a well-defined quantity for any particular Auger emission. It should be noted that in the Auger process deexcitation and electron emission are events that take place simultaneously due to the electron-electron interaction.

The processes of interest here, namely DR and RTE, take place via the time reversed Auger mechanism. A schematic of the formation of the intermediate state in dielectronic recombination is shown in Figure 2, where the

"wavy" line represents the interaction which takes place. It is noted that the DR process includes, by definition, subsequent emission of the deexcitation photon as well.

Comparing Figures 1 and 2, we can see that DR proceeds through the time reversed Auger process. It was mentioned before that the kinetic energy of the Auger electron has only discrete values, and since DR is the time-reversed Auger process, it, too, depends upon the energy difference between the initial and final states of the projectile ion. This means that, in the rest frame of the ion, the energy of the colliding electron must equal the corresponding Auger energy for the transition to take place. Therefore, resonance conditions in DR occur when the relative velocity of the projectile ion and the target electron corresponds to the velocity of the Auger electron that would be ejected as a result of the decay of the doubly-excited state of the ion. The principal difference between DR and RTE is that for the latter process the captured electron is initially (weakly) bound in a target. Theoretical calculations of the DR cross sections have been done (Roszman, 1979; McLaughlin and Hahn, 1982; Nasser and Hahn, 1983) during the last years and these cross sections, together with the momentum distribution of the target atoms (see below), are used in the theoretical calculations of the RTE cross sections.

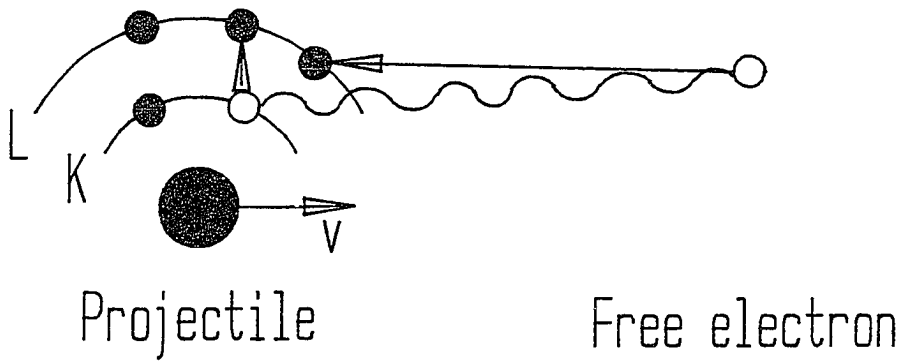

Figure 2. Schematic of the Formation of the Doubly-Excited Intermediate Resonant State in Dielectronic Recombination for a Li-Like Ion Colliding With a Free Electron.

A process which competes with RTE (i.e., it gives rise to the same intermediate states) is nonresonant transfer and excitation (NTE). A schematic of the NTE process is shown in Figure 3, again for a Li-like ion with the "wavy" lines representing the interactions. Referring to this figure we see that NTE is a two-step process which can give rise to the same intermediate excited states as RTE. The formation of the intermediate excited state occurs first by excitation of a projectile electron through the Coulomb interaction with the target nucleus and, second, by capturing an electron from the target atom. The capture and excitation events are independent and therefore no resonant conditions are involved in NTE.

Since NTE is a two-step process (excitation followed

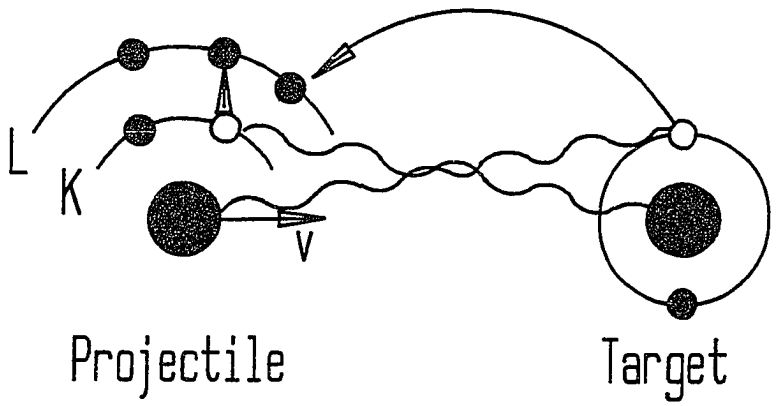

Figure 3. Schematic of the NTE Process for a Li-Like Ion.

by capture) the NTE cross section depends on both excitation and capture cross sections. Mathematically the NTE cross section is given by the expression:

$$\sigma_{NTE} = \int_0^\infty 2\pi P_K^{excit}(b)\, P_L^{capture}(b)\, b\,db \qquad (2.2)$$

where b is the collision impact parameter, P_K^{excit} (b) is the K-shell excitation probability of the ion, and $P_L^{capture}$ (b) is the capture probability of a target electron to the L shell of the ion. Over the range of b where P_K^{excit} (b) is nonzero, $P_L^{capture}$ (b) is approximately constant (Pepmiller, 1983) and equal to $P_L^{capture}$ (o) (i.e., the probability for zero impact parameter). Therefore:

$$\sigma_{NTE} = 2\pi P_L^{capture}(o) \int_o^\infty P_K^{excit}(b)\, b\,db \qquad (2.3)$$

Since

$$\sigma_K^{excit} = 2\pi \int_0^{\infty} P_K^{excit}(b)\, b db \qquad (2.4)$$

the former expression becomes:

$$\sigma_{NTE} = P_L^{capture}(o) \cdot \sigma_K^{excit} \qquad (2.5)$$

In Figure 4, σ_{NTE} is schematically shown. Thus the NTE cross sections can be predicted by using the K-shell excitation cross sections and the probability of electron capture to the L-shell of the ion for small impact parameters.

The projectile energy dependence of the NTE peak will vary depending upon the charge state of the projectile and upon the atomic number of the target. NTE is generally expected to be dominant at projectile energies lower than those for which RTE occurs (Feagin et al., 1984; Tanis et al., 1985; Reeves et al., 1985; and Swenson et al., 1986).

A final process which competes with RTE is two electron transfer and excitation (2eTE). A schematic of the 2eTE process is shown in Figure 5. Referring to this figure, we see that 2eTE is also a two-step process, like NTE, but here the excitation is not due to an interaction with the target nucleus but with a second target electron.

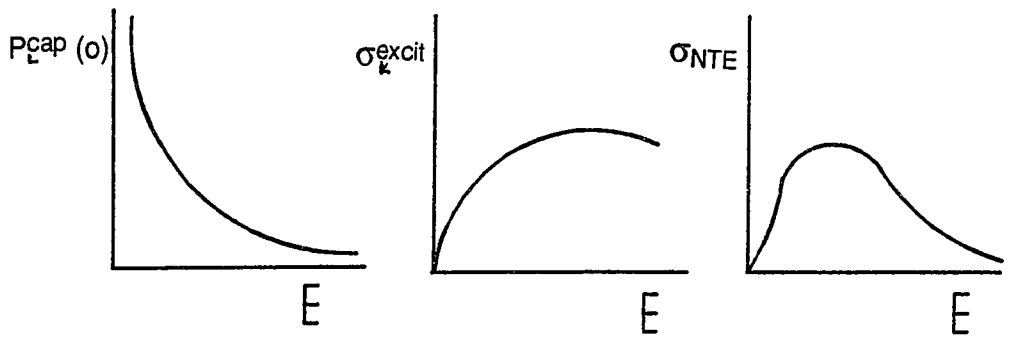

Figure 4. Schematic of the NTE Cross Section Curve as a Product of the L-Shell Capture Probability and K-Shell Excitation Cross Section Curves.

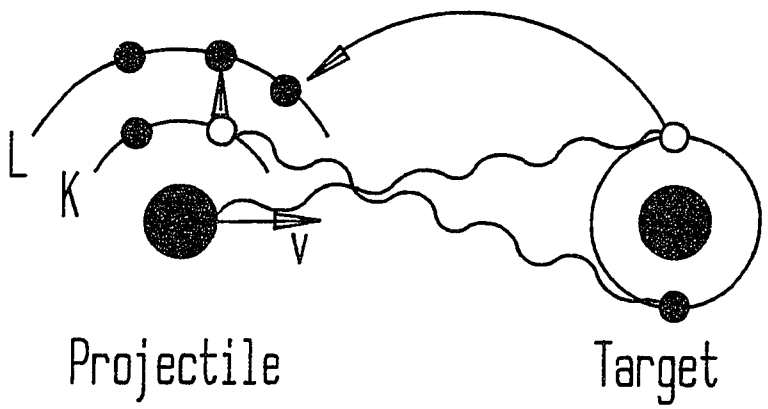

Figure 5. Schematic of the 2eTE Process for a Li-Like Ion.

Unfortunately, there are no accurate numerical calculations yet available for 2eTE cross sections. Rough estimates of 2eTE cross sections (Schulz et al., 1988) are made using calculated cross sections for excitation by free electrons

(Bhatia and Temkin, 1977) and Oppenheimer-Brinkman-Kramers capture probabilities.

Let us now focus on RTE itself which, as already mentioned, is very similar to DR. RTE occurs in an ion-atom collision when simultaneous excitation of the ion and capture of a target electron are followed by relaxation which results in x-ray or electron emission. It is important to note that the excitation and capture occur (see Figure 1) only when the relative velocity of the projectile ion and the incoming electron matches the velocity of the ejected Auger electron in the inverse process for the resonance state formed. Referring to Figures 1 and 2, we can see that the only difference between RTE and DR is the initial state of the target electron, i.e., for RTE the electron is bound, while for DR the electron is free.

The theoretical formulation of RTE (Brandt, 1983) is based on the impulse approximation, which states that immediately after the collision the separation between the projectile and target is such that no further interaction can take place. In order to satisfy the impulse approximation, the velocity of the ion must be much greater than the velocity of the captured target electron (i.e., $V_{ion} >> V_{electron}$). The RTE energies for the systems considered here (on the order of K-shell excitation energies) satisfy

this criterion for the weakly bound electrons of H_2 or He. Therefore, the theoretical interpretation of RTE is given by approximating a collision between an ion and a free electron. Of course, many intermediate resonance states are possible in the RTE process but here we focus only on those transitions in which at least one of the active electrons involved in the RTE process occupies a level in the intermediate state with principal quantum number n = 2 (i.e., a K-shell electron of the projectile is promoted to the L-shell simultaneous with the capture of a target electron to $n \geq 2$).

In the impulse approximation, RTE is equivalent to dielectronic recombination averaged over the electron momentum distribution of the target electrons and the cross section is given by:

$$\sigma_{RTE} \sim \sigma_{DR} \sum_i J_i(P_{iz}) \qquad (2.6)$$

where σ_{RTE} is the RTE cross section, σ_{DR} is the DR cross section and $J_i(P_{iz})$ is the Compton profile (momentum distribution) of the target electron (i.e., the probability of finding a particular target electron with momentum component P_{iz} along the beam axis). The DR cross sections are in general difficult to calculate, but the results for several ions have been reported to date. In this thesis,

the RTE measurements presented are compared with calculations based on Equation (2.6).

The Compton profile term results from the fact that the electrons available for capture are bound to the nucleus of the target atom. Calculated Compton profiles of all atoms have been tabulated (Biggs, Mendelson, and Mann, 1975) from numerical calculations based on Hartree-Fock wave functions. The Compton profile for the electrons in a neutral, ground state atom is a symmetric Gaussian function of momentum, p, centered about p=0. A graphical representation of the Compton profile for H_2 is given in Figure 6, where $J_i(P_{iz})$ is the probability momentum distribution function of the target electron and P_{iz} is the z component of the momentum of the i^{th} electron in the target. In Equation (2.6), the Compton profile is summed over all electrons which can contribute to the formation of the specific intermediate state.

Referring to Figure 6 we can see that in the laboratory rest frame the target electron is most likely to have a zero momentum component along the beam axis (z axis). In addition to that, the Compton profile for the electrons in any given atom is a continuous function of momentum. Therefore, a range of relative velocities between the projectile and the target electron satisfy the resonance condition (i.e., equal to the Auger electron

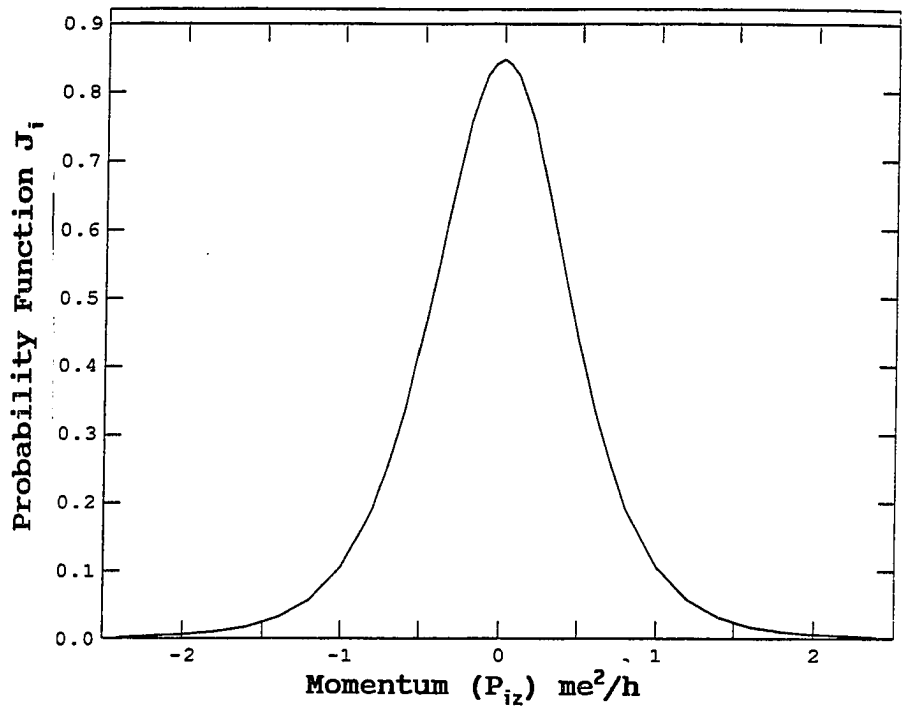

Figure 6. Graphical Representation of the Compton Profile for H_2.

velocity), and there is a nonzero probability that an intermediate resonance state of RTE will be formed. Since these states are identical to the resonance states of DR, the Compton profile term in Equation (2.6) broadens the sharply defined DR peak which corresponds to the particular resonance state formed. The extent to which the peak is broadened is proportional to the width of the Compton profile.

In the rest frame of the ion, the momentum of the i^{th} electron along the beam axis is given by (Brandt, 1983):

$$P_{iz} = \left(K - \frac{Em}{M}\right)\left(\frac{M}{2E}\right)^{1/2} \qquad (2.7)$$

Where K is the corresponding Auger energy for the (intermediate state) transition that takes place, E is the projectile energy, m is the mass of the electron and M is the mass of the projectile ion.

For $P_{iz} = 0$ (the Compton profile has its maximum at $P_{iz} = 0$) Equation (2.7) implies that:

$$E = \frac{KM}{m} \qquad (2.8)$$

Equation (2.8) simply transforms the position of each broadened peak from the Auger energy to the laboratory frame projectile energy.

We can now summarize the effect of Equation (2.6) by saying that a DR resonance is broadened by having the target Compton profile superimposed upon it, and then transformed to the projectile lab frame energy. This is done for each of the DR peaks representing different intermediate excited states. The contributions due to each peak are added together to obtain the total RTE cross section. As an example, Figure 7 shows the measured cross sections (Tanis et al., 1984) for 100-360 MeV Ca^{17+} + He along with the calculated RTE cross sections and the

theoretical positions and relative intensities of the intermediate states for dielectronic recombination.

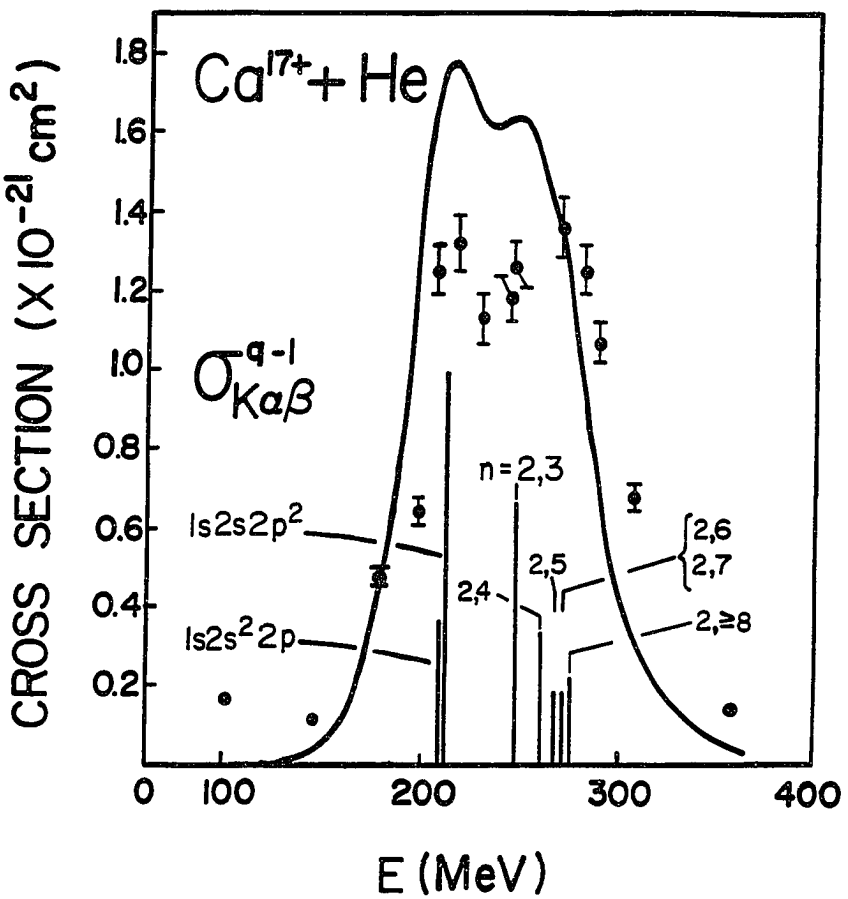

Figure 7. Measured Cross Sections for Electron Capture Coincident With K x-ray Emission, (Tanis et al., 1984) in 100-360 MeV Ca^{17+} + He Collisions Along With the Calculated RTE Cross Sections (Solid Line) and the Theoretical Positions and Relative Intensities of the Intermediate Doubly-Excited States for Dielectronic Recombination.

CHAPTER III

EXPERIMENT

Motivation

Measurements of resonant transfer and excitation (RTE) were made at the Oak Ridge National Laboratory (Schulz et al., 1988) for 15-33 MeV F^{6+} (Li-like) ions colliding with H_2. The magnitude of the measured RTE cross sections was found to be nearly a factor of two smaller than theory (Bhalla and Karim, 1989; Badnell, 1990) and, furthermore, it was suggested that a substantial contribution to the cross section on the high-energy side of the resonant maximum, which could not be attributed to RTE, was instead due to the two-electron-transfer and excitation process (2eTE) (see Figure 8). It should be noted that the contribution from this latter process is expected to be small compared to the RTE mechanism (Schulz et al., 1988).

In order to investigate RTE for this system more completely, we undertook similar measurements at Western Michigan University (Kalamazoo) using the EN tandem Van de Graaff accelerator. In addition, related measurements were made for $F^{q+} + H_2$ and F^{q+} + He collision systems with q = 6,8,9. Both the Oak Ridge data as well as theoretical

calculations are compared with the present data.

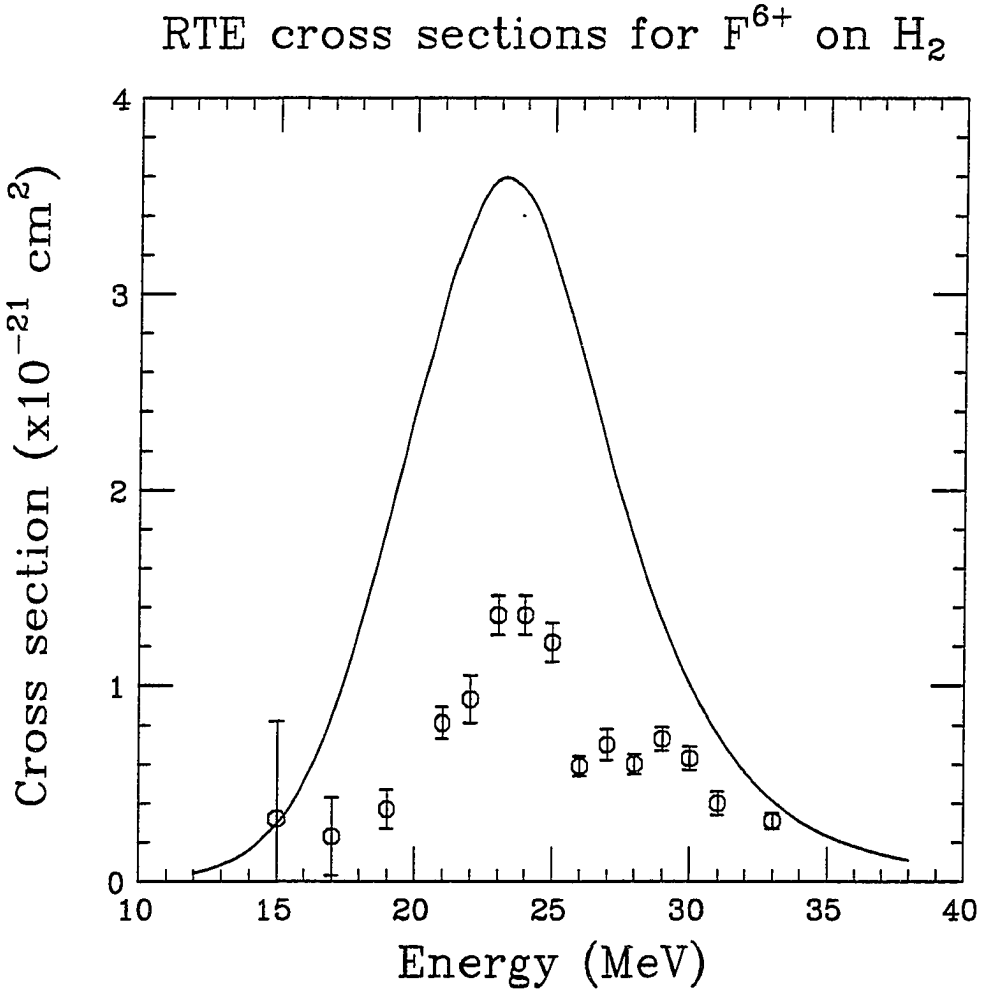

Figure 8. RTE Cross Sections for F^{6+} + H_2 Measured at the Oak Ridge National Laboratory (Schulz et al., 1988).

The solid curve is the calculated RTE cross section (Bhalla,1989).

Description of the Experimental Arrangement

A projectile beam composed of F^{q+} ions was accelerated and directed into a gas cell containing the H_2 target atoms. As the projectile goes through the target gas cell, it can interact with a target atom and form the intermediate state characteristic of RTE or one of the nonresonant NTE or 2eTE processes. The excited state can then decay by emitting a K x ray. Since the formation of the intermediate state requires the capture of a target electron by the ion, the projectile ion becomes less positive (i.e., $q \rightarrow q-1$), and can be detected by magnetic separation of the charge-changed components of the projectile beam emerging from the gas cell. By collecting the charge-changed components and the non-charge-changed component we can determine the fraction of projectile ions that have undergone capture. But in order to determine that an intermediate excited state characteristic of RTE, NTE, or 2eTE has been formed we also need to detect the K x ray which results from the relaxation of the excited state (see Figure 1). In this experiment, detection of a K x ray ($K\alpha$ for $n = 2 \rightarrow n = 1$ and $K\beta$ for $n \geq 3 \rightarrow n = 1$) implies excitation of a K-shell electron in the projectile ion. Since a Li-like ion has two electrons initially in the K-shell, the only way K x-ray emission can occur is if one of the two K-shell

electrons is promoted to a higher shell or removed from the ion.

A schematic of the beam line apparatus is shown in Figure 9. Two sets of slits (only one set shown) were used to collimate the incident beam; a Si(Li) x-ray detector viewed the interaction region (the target gas cell) at an angle of 90 degrees to the beam axis; the beam components were separated by a magnet; finally, a solid-state detector was used to detect the charge-changed (single capture) beam component while a Faraday cup was used to collect the main beam component.

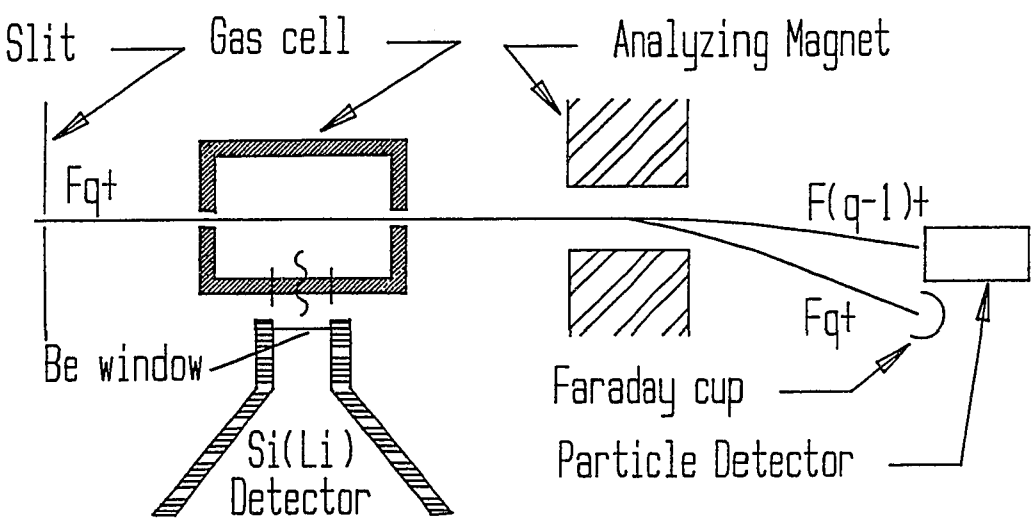

Figure 9. Schematic of the Experimental Apparatus.

A schematic of the electronics is shown in Figure 10. Signals from the Si(Li) detector were routed through a Timing Filter Amplifier (TFA) and a Constant Fraction Discriminator (CFD), which converts the analog x-ray signal into a logic signal when the amplitude of the x-ray pulse exceeds the discriminator level. The logic signal from the CFD provided the START signal for a Time-to-Amplitude Converter (TAC) and a similar set of electronics from the particle detector provided the STOP signal. The TAC then gives an analog output pulse whose amplitude is proportional to the time difference between the START and the STOP signals. A TAC output occurs any time an x-ray event and a capture event are detected within a preset time period (2μsec in this case). In this way a time spectrum is constructed for each run (i.e., coincidence counts versus time). In addition, the total x-ray emission spectrum (number of x-ray events versus x-ray energy) was recorded as was the total number of capture events. A typical K x-ray spectrum corresponding to total K x-ray emission as well as time spectrum corresponding to K x-ray emission coincident with capture are shown in Figure 11. All of the data were collected and sorted using a μVAX II computer which was interfaced to the signal processing electronics.

The coincidence spectra were generated from software

sorting routines in the data acquisition program. These sorting routines are used to associate x-ray events with coincidence events from the TAC, thereby producing an x-ray coincidence spectrum. Data were collected for a specific target cell gas pressure, and several different pressure runs were conducted at each projectile energy in order to verify the linear dependence of the charge-changed and x-ray event fractions with respect to the gas cell pressure. This is necessary since linearity ensures that single-collision conditions prevail. Three runs for each projectile energy (e.g., pressures of 0, 50, 80 mTorr) were conducted in the energy range of 16.5 - 38 MeV (F^{6+} + H_2). The total number of x-ray and coincidence counts were obtained by integrating the region of interest (the peak region in Figure 11) of each spectrum. By plotting the yield (i.e., number of counts/number of incident ions) of x-ray and coincidence counts versus the gas cell pressure, one can verify the linear dependence of the measured yields with respect to the gas cell pressure (see Figure 12).

The same experimental set-up was used in order to perform the F^{q+} + He and F^{q+} + H_2 measurements (q=6,8,9). In the next chapter the results of all the experimental work are presented.

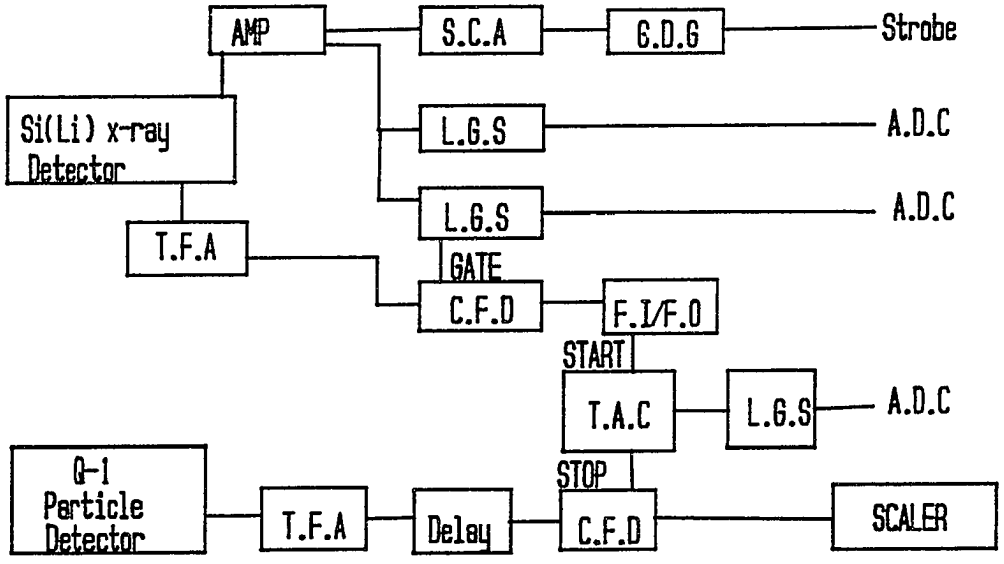

Figure 10. Schematic of Electronics for Signal Processing.

Key to Abbreviations

T.F.A.	=	Timing Filter Amplifier
C.F.D.	=	Constant Fraction Discriminator
S.C.A.	=	Single Channel Analyzer
G.D.G.	=	Gate and Delay Generator
L.G.S.	=	Linear Gate Stretcher
T.A.C.	=	Time-to-Amplitude Converter
F.I./F.O.	=	Logic Fan in/Fan out
A.D.C.	=	Analog/Digital Converter

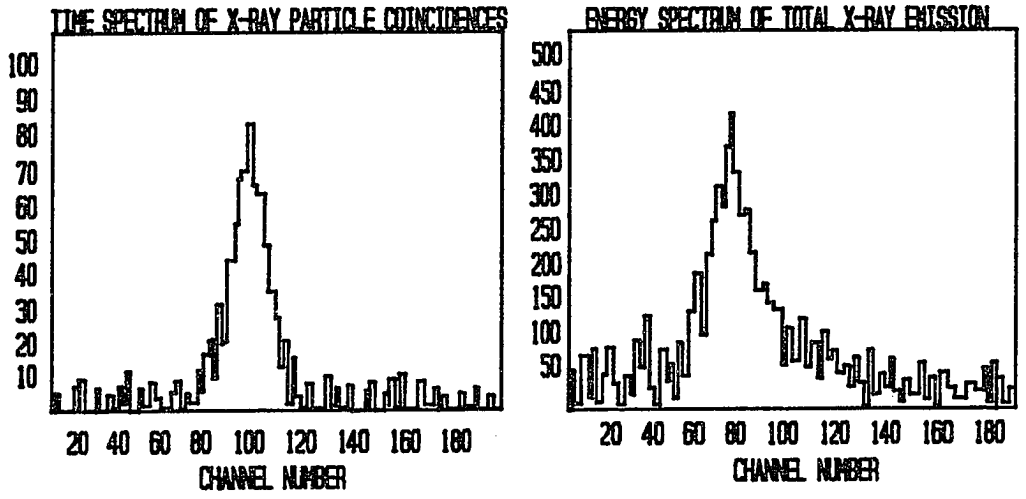

Figure 11. Typical TAC and x-ray Spectra.

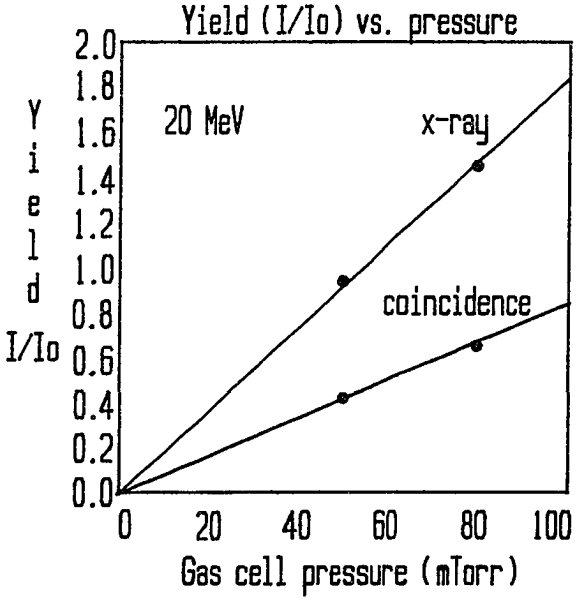

Figure 12. Plots of the Yield of Total x-ray and Coincidence (x-ray and Capture) Yields Versus the Gas Cell Pressure for F^{6+} + H_2 at 20 MeV.

CHAPTER IV

DATA ANALYSIS AND RESULTS

Determination of Cross Sections

The number of x rays which are detected (see Chapter III) depends on the integrated incident beam intensity, the thickness of the target, the geometry of the gas cell, the total x-ray cross section, the efficiency of the x-ray detector, and the solid angle subtended by the detector. Mathematically the number of observed events is given by:

$$I_x = I_o t \, \sigma_x \epsilon_x \left[\frac{\Delta \Omega_x}{4\pi} \right] \qquad (4.1)$$

Where:

- I_x is the number of x-ray events,
- I_o is the total number of incident ions that pass through the target cell,
- σ_x is the x-ray cross section,
- ϵ_x is the efficiency of the x-ray detector,
- $\Delta\Omega_x$ is the solid angle subtended by the x-ray detector,
- t is the target thickness in atoms/cm^2 and is equal to the quantity $N_o PL$,
- N_o is a constant (3.3×10^{13} atoms/cm^3mTorr),
- P is the gas cell pressure in mTorr,

L is the effective length of the gas cell in cm,

Using the quantity N_oPL as target thickness and dividing through by I_o Equation 4.1 becomes:

$$F_x = \frac{I_x}{I_o} = \sigma_x\left[\epsilon_x N_o L\left(\frac{\Delta\Omega_x}{4\pi}\right)\right]P \qquad (4.2)$$

$$F_x = \sigma_x\left[\frac{1}{\delta}\right]P \qquad (4.3)$$

where F_x is the fraction of the x rays that are detected, and δ is a constant that depends on the geometry of the gas cell, the efficiency of the x-ray detector, and the solid angle subtended by the detector. Since σ_x is a constant, Equation 4.3 implies that F_x depends linearly on P. For each incident projectile energy, several pressure runs were performed (each run at a well-defined gas cell pressure), and therefore the linear dependence of F_x versus P was established for each projectile energy (see Figure 12).

According to Equation 4.3, the slope of the resulting straight line is equal to the coefficient of P:

$$\frac{\Delta F_x}{\Delta P} = \frac{\sigma_x}{\delta} \qquad (4.4)$$

Therefore, finding the slope that corresponds to each projectile energy value provides a means of finding the x-

ray cross section at that energy:

$$\sigma_x = \delta\left(\frac{\Delta F_x}{\Delta P}\right) \qquad (4.4')$$

By following similar procedures, we can get expressions for both the coincidence and capture cross sections:

$$\sigma^x_{q-1} = \delta\left(\frac{\Delta F^x_{q-1}}{\Delta P}\right) \qquad (4.5)$$

$$\sigma_{q-1} = \delta'\left(\frac{\Delta F_{q-1}}{\Delta P}\right) \qquad (4.6)$$

where σ^x_{q-1} and σ_{q-1} are the coincidence and total capture cross sections respectively. In Equation 4.6, δ' is not the same as δ in Equations 4.4' and 4.5 since capture detection does not require the use of an x-ray detector. In this case, δ' is simply equal to:

$$\delta' = \frac{1}{(N_o L)} \qquad (4.7)$$

It should also be noted that δ for x-ray emission (Equations 4.4' and 4.5) will vary with the charge state since δ depends on ϵ_x which in turn is a strong function of x-ray energy for the relatively low energy x-ray energies

investigated here. Because the different charge states emit x rays of slightly different energies, ϵ_x will vary significantly.

The determination of the cross section of course requires that δ itself has to be known. There are three procedures one may follow in order to determine δ. First of all, δ can be calculated directly (see Equations 4.2 and 4.3) if the length of the gas cell, the efficiency, and the solid angle subtended by the x-ray detector are known. In this experimental work, all of the above mentioned quantities were measured and the resulting calculated value (Clark, 1989; Bernstein, 1990) of $\delta(5+) = 69.4X10^{-12}$ cm^2 mTorr is shown graphically in Figure 13.

The quantity δ can also be determined by normalizing to known cross sections (i.e., in this case, total x-ray emission) determined previously by another experimental team. To accomplish this normalization, some data were taken for F^{6+} projectiles colliding with He since this same measurement was performed in 1979 at Kansas State University (Tawara et al., 1979). If σ_x is the total x-ray production cross section, then for a given projectile energy value:

$$\sigma_x^{present}(6+) = 1.23\sigma_x^{KSU}(6+) \qquad (4.8)$$

The factor 1.23 is used in order to account for higher

energy x rays which were not considered in the Kansas State University measurements (Bernstein, 1991). However, the cross sections for x rays coincident with capture for incident F^{6+} ions are in fact due to the decay of F^{5+} projectile ions (Bernstein, 1990) since during the RTE process the projectile ion captures a target electron and so its charge state is reduced by one unit. For incident F^{6+} most of the x-ray emission results from excitation and excitation accompanied by electron loss. Thus, the emitted x rays are from charge states higher (i.e., 6+, 7+, and 8+) than that of the F^{5+} ions which result from the RTE process.

A correction for the relative absorption of F^{5+} RTE x rays compared to F^{6+} total emission x rays must be made to obtain the correct normalization for the RTE cross sections.

Using Equations 4.2 and 4.3, we have:

$$\delta(5+) = \frac{4\pi}{\epsilon_x(5+)\Delta\Omega_x N_o L} \qquad (4.9)$$

$$\delta(6+) = \frac{4\pi}{\epsilon_x(6+)\Delta\Omega_x N_o L} \qquad (4.10)$$

Equations 4.9 and 4.10 give:

$$\delta(5+) = \delta(6+)\frac{\epsilon_x(6+)}{\epsilon_x(5+)} \qquad (4.11)$$

The ratio of $\epsilon_x(6+)/\epsilon_x(5+)$ is calculated to be 1.48 (Bernstein, 1990, private communication). Therefore, Equation 4.11 becomes:

$$\delta(5+) = 1.48\delta(6+) \qquad (4.12)$$

where $\delta(6+)$ can be determined by using Equations (4.8) and (4.4'):

$$\delta(6+) = \frac{1.23\sigma_x^{KSU}(6+)}{\left(\frac{\Delta F_x(6+)}{\Delta P}\right)^{present}} \qquad (4.13)$$

Equations 4.11 and 4.13 were then used for three projectile energy values (20, 24, 32 MeV) to obtain values of $\delta(5+)$ as shown graphically in Figure 13.

Finally, δ was also determined from data that were taken for bare F projectiles colliding with H_2. Except for capture to the K-shell or to metastable states, each incident projectile ion which emerges from the target with a charge reduced by one unit (i.e., F^{8+}) should lead to a K x ray, so that

$$\sigma_{capture} \simeq \sigma_x(8+) \qquad (4.14)$$

where $\sigma_x(8+)$ is the K x-ray emission cross section from F^{8+} following capture by F^{9+}. Since it is estimated that

capture to the K-shell and to metastable states is about 10% of the total capture (Schulz et al., 1988) Equation 4.14 becomes:

$$0.9\sigma_{capture} = \sigma_x(8+) \qquad (4.15)$$

Using Equations (4.15) and (4.4') $\delta(8+)$ can be determined:

$$\delta(8+) = \frac{0.9\sigma_{capture}}{\left(\frac{\Delta F_x(8+)}{\Delta P}\right)} \qquad (4.16)$$

But a correction factor is again needed in order to correct for the relative absorption of F^{5+} RTE x rays compared to the x rays emitted from F^{8+}. An equation similar to (4.11) gives:

$$\delta(5+) = \delta(8+)\frac{\epsilon_x(8+)}{\epsilon_x(5+)} \qquad (4.17)$$

The ratio $\epsilon_x(8+)/\epsilon_x(5+)$ (i.e., correction factor) is calculated (Bernstein, 1990) to be 3.72 so that

$$\delta(5+) = 3.72\delta(8+) \qquad (4.18)$$

Equations 4.16 and 4.18 were then used for two projectile energy values (30, 34, MeV) and the resulting values of

$\delta(5+)$ are shown in Figure 13.

Figure 13 is the graphical representation of the values of $\delta(5+)$ which were obtained by following the above three mentioned procedures. By referring to that figure one may observe that all the values of $\delta(5+)$ are in reasonable agreement with each other. The value of $\delta(5+)$ used to determine the RTE cross sections for F^{6+} on H_2 is the calculated one (see Figure 13).

As a final note, the F^{q+} on He measurements (q = 8,9) were performed using a different gas cell geometry than the one used for the F^{6+} on H_2 measurements. Using that geometry, some additional data (20, 24 MeV) were taken for F^{6+} ions colliding with He in order to be able to determine δ for this case as well.

At this point, both the coefficients (δ) and the slopes are known and therefore by using Equations 4.4', 4.5, and 4.6, the cross sections for x rays coincident with capture, total x-ray emission and total capture can be determined. The values of δ used to obtain the various x-ray cross sections are shown in Table 1.

Table 1

Values of δ ($10^{-12}cm^2$ mTorr) Used to Calculate the Total (σ_x) and Coincidence (σ^x_{q-1}) x-ray Cross Sections

Target	H_2		He	
Projectile	σ_x	σ^x_{q-1}	σ_x	σ^x_{q-1}
F^{6+}	46.9	69.4	46.9	69.4
F^{8+}	31.2	31.2	66.1	66.1
F^{9+}	18.7	18.7	32.9	32.9

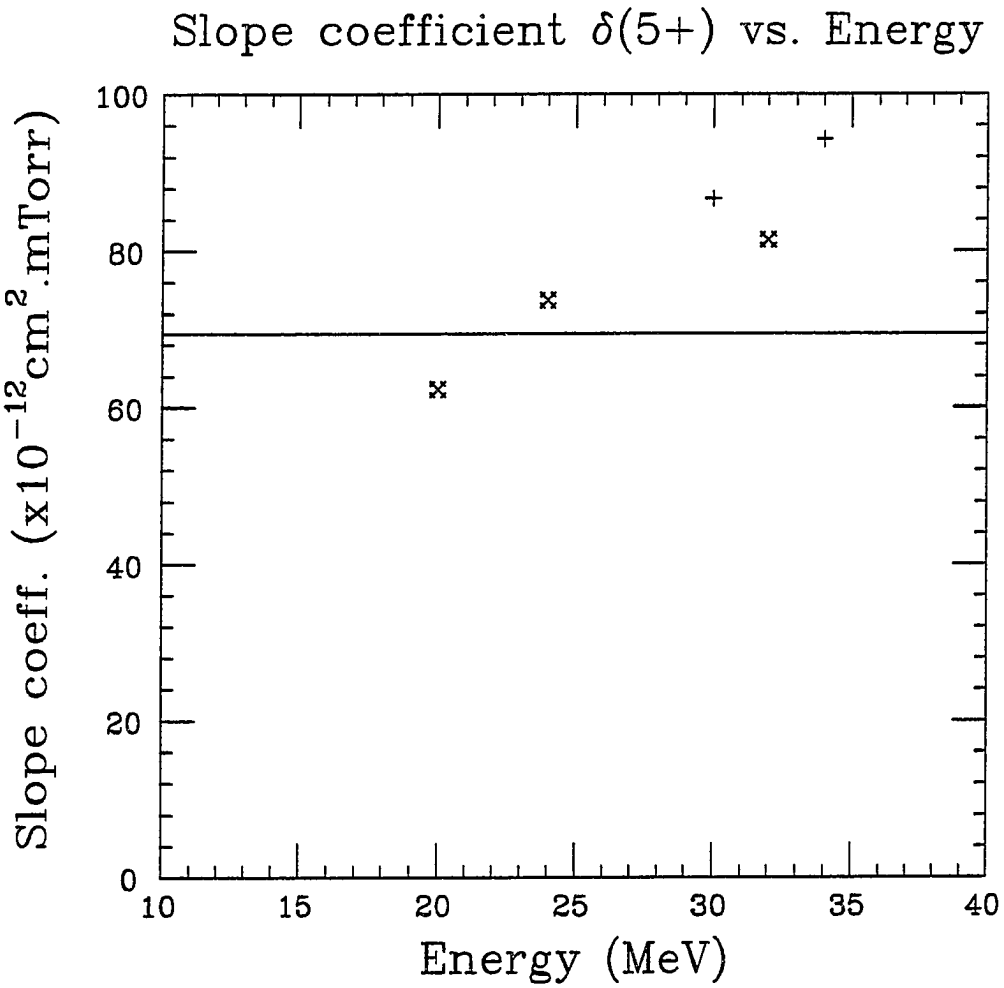

Figure 13. Graphical Representation of the Obtained Values of $\delta(5+)$ (i.e.,Inverse of the Product of Detector Efficiency, Target Length and Solid Angle).

The horizontal line represents the calculated value (see Equations 4.2 and 4.3); the stars represent the values of $\delta(5+)$ obtained by using the normalization technique of Equation 4.8 and the crosses represent the value of $\delta(5+)$ obtained by using the normalization technique of Equation 4.15.

Results

The results obtained from the experimental work described in this thesis are presented in Figures 14 through 22. Figure 14 shows the measured cross sections for single electron capture and simultaneous emission of a K x ray versus projectile energy for the $F^{6+} + H_2$, $F^{8+} + H_2$ and $F^{9+} + H_2$ systems. The error bars shown are only statistical uncertainties. The systematic uncertainties giving rise to the uncertainties in δ (see Table 1) are estimated to be about 30%. For the $F^{6+} + H_2$ data there is a maximum at about 25 MeV whereas the F^{8+} data decrease monotonically with beam energy. The vertical arrows along the energy axis indicate projectile energies for which RTE resonances are expected for the $F^{6+} + H_2$ system. Auger notation is used for the intermediate states populated; e.g., KLL means a K electron is excited to the L shell and an electron is also captured to the L shell.

It should be noted that, in addition to RTE, the competing process of NTE (see Chapter II) followed by x-ray emission can contribute to the measured cross sections for capture coincident with emission of an x ray. Theoretical estimates of the NTE cross sections (Brandt, 1983) show that its projectile energy dependence should be different from that of the RTE cross sections (Pepmiller et al.,

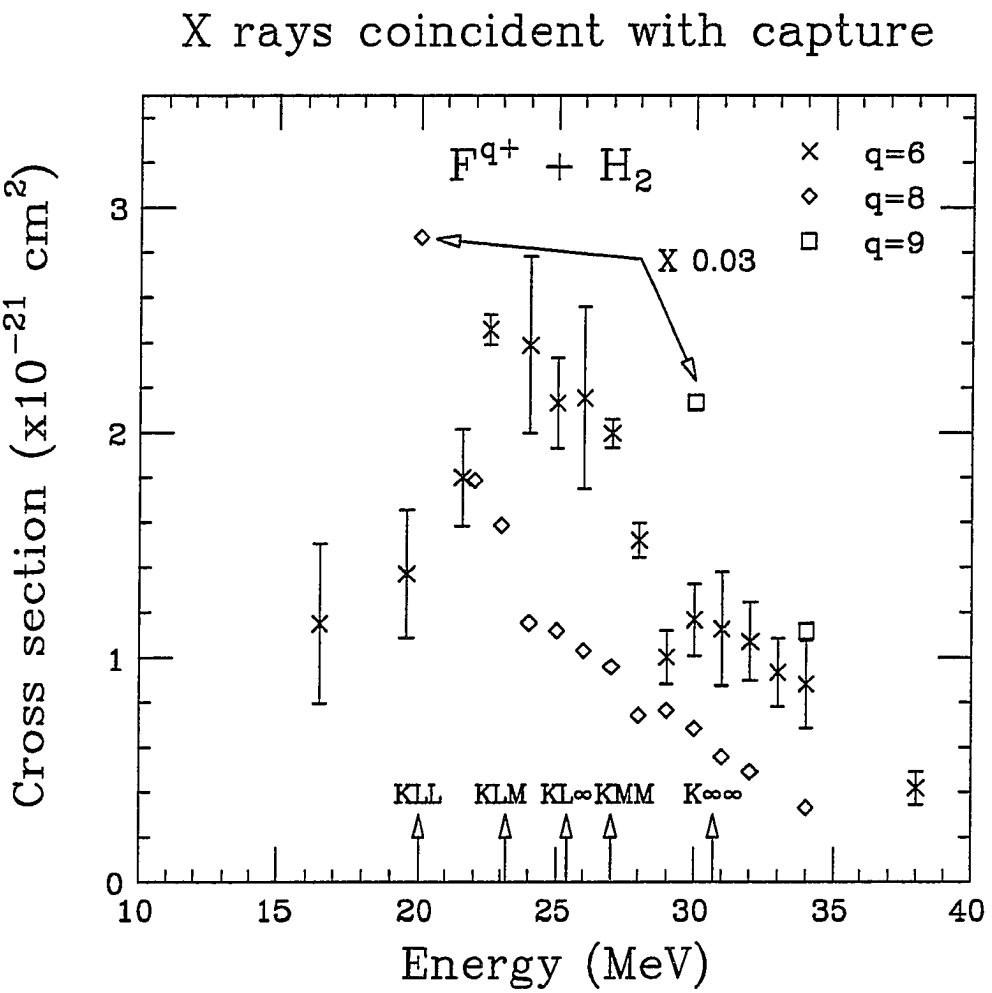

Figure 14. Measured Cross Sections for Single Electron Capture Coincident With K x-ray Emission Versus Projectile Energy for $F^{6+} + H_2$, $F^{8+} + H_2$ and $F^{9+} + H_2$.

The vertical arrows along the energy axis indicate the resonance energies for some intermediate states of the DR process for the $F^{6+} + H_2$ system.

Table 2

Cross Sections for Single Electron Capture Coincident With K x-ray Emission for $F^{q+} + H_2$

q	Energy (Mev)	σ^{x}_{q-1} ($x10^{-21}cm^2$)	Uncertainty ($x10^{-21}cm^2$)
6	16.5	1.15	0.49
6	19.5	1.37	0.50
6	21.6	1.80	0.58
6	22.6	2.39	0.74
6	24	2.46	0.82
6	25	2.13	0.67
6	26	2.15	0.76
6	27	2.00	0.60
6	28	1.52	0.46
6	29	1.00	0.32
6	30	1.17	0.38
6	31	1.13	0.42
6	32	1.07	0.36
6	33	0.93	0.32
6	34	0.88	9.33
6	38	0.42	0.14
8	20	95.6	28.8
8	22	59.6	18.0
8	23	52.9	16.0
8	24	38.4	11.6
8	25	37.3	11.3
8	26	34.4	10.4
8	27	32.0	9.66
8	28	24.8	7.57
8	29	25.5	7.70
8	30	22.8	6.89
8	31	18.6	5.63
8	32	16.4	4.98
8	34	11.0	3.37
9	30	71.1	21.4
9	34	37.2	11.2

1985), and the NTE maximum is expected to occur at energies lower than the RTE resonance energies. For F^{6+} + H_2, the NTE maximum should be at about 8 MeV. On the low-energy side of the NTE maximum, the cross section decreases steeply. The high-energy side, however, displays a much slower decline giving rise to a strongly asymmetric and much broader maximum than the RTE resonances. Such a projectile energy dependence was observed for the collision system S^{13+} + He (Tanis et al., 1985).

The projectile energy dependence of the present F^{6+} + H_2 data (see also Figure 16) indicates that the observed maximum is due to RTE. The maximum corresponds nearly to the average position of the resonance energies for populating KLn ($n \geq L$) states by RTE, and it has a shape that is quite symmetric. Furthermore, according to theory (Brandt, 1983), the contribution from NTE for this system should be < 5% in the region of the RTE maximum.

The contribution to the cross section on the high-energy side of the resonant maximum (≥ 30 MeV) is above the KLn series limit and at present the origin of this high-energy contribution is not completely clear since the energy range for this contribution coincides with the resonance energies for populating Knm ($n, m > L$) states by RTE. Generally, the intensities of these transitions compared to the KLn transitions are expected to be

negligible (Bhalla, 1989; Badnell, 1990).

In the $F^{8+} + H_2$ data, no clear structure can be seen. The cross sections for capture and simultaneous emission of an x ray decrease as the projectile energy increases, a feature that is characteristic of the capture probability function. This behavior is expected since an F^{8+} ion has only one electron in the K shell and, therefore, except for capture to the K-shell and population of metastable states, each projectile with a charge reduced by one unit (i.e., a capture event) should lead to a K x-ray event. It is obvious for the same reason that capture is the only mechanism responsible for K x-ray emission from an incident bare F ion. The two $F^{9+} + H_2$ data points clearly justify the above hypothesis for this system as well.

Figure 15 shows the measured cross sections for total K x-ray production versus projectile energy for $F^{6+} + H_2$, $F^{8+} + H_2$ and $F^{9+} + H_2$. In the $F^{6+} + H_2$ data the total K x-ray emission cross section curve has the shape characteristic of an excitation cross section for the projectile energies used. Since for a F^{6+} projectile ion, K-shell excitation gives rise to x-ray emission, the x-ray emission cross section curve is expected to have the shape of the K-excitation cross section. At low energies, the probability for a K-shell electron to be excited to a higher shell (and then decay back to the K-shell by emitting an x ray) is

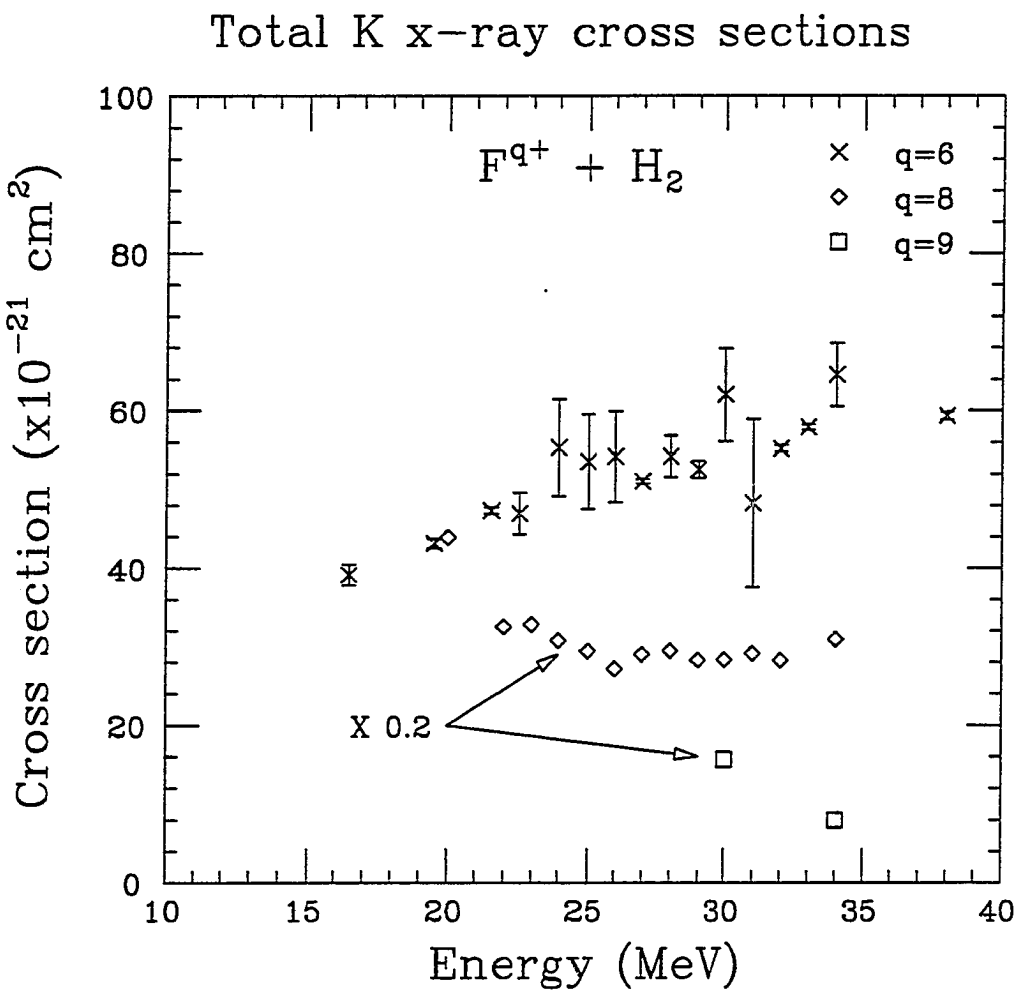

Figure 15. Measured Cross Sections for Total K x-ray Production Versus Projectile Energy for F^{6+} + H_2, F^{8+} + H_2 and F^{9+} + H_2.

Table 3

Cross Sections for Total K x-ray Production for $F^{q+} + H_2$

q	Energy (Mev)	σ_x(x10^{-20}cm^2)	Uncertainty(x10^{-20}cm^2)
6	16.5	3.92	1.18
6	19.5	4.32	1.30
6	21.6	4.73	1.42
6	22.6	4.70	1.43
6	24	5.53	1.77
6	25	5.35	1.71
6	26	5.42	1.72
6	27	5.10	1.53
6	28	5.42	1.65
6	29	5.25	1.58
6	30	6.20	1.95
6	31	4.82	1.80
6	32	5.51	1.65
6	33	5.78	1.73
6	34	6.46	1.98
6	38	5.93	1.78
8	20	22.0	6.60
8	22	16.3	4.89
8	23	16.4	4.93
8	24	15.4	4.62
8	25	14.7	4.42
8	26	13.6	4.08
8	27	14.5	4.36
8	28	14.7	4.43
8	29	14.1	4.24
8	30	14.2	4.25
8	31	14.6	4.37
8	32	14.1	4.24
8	34	15.5	4.64
9	30	7.81	2.45
9	34	3.99	1.20

very small. As the projectile energy increases the excitation probability increases and is expected to reach a maximum near 35 MeV (i.e., the energy at which $V_{ion}=V_{electron}$) (Khandelwal et al., 1969).

For F^{8+} + H_2, either excitation (1s -> 2p) or capture (to levels n ≥ 2) may give rise to K x-ray emission. At low energies, capture will dominate while at high energies excitation will dominate. The maximum in the excitation cross section should occur near 38 Mev (Khandelwal et al., 1969). But the the x-ray cross sections for F^{8+} are considerably larger than those for F^{6+}, even at relatively high energies, indicating that these x rays may be the result of both electron capture and electron excitation. The F^{9+} + H_2 data show that the cross section values for total K x-ray production decrease as the projectile energy increases, something that is expected since capture is the only process leading to x-ray emission here.

Figure 16 shows the calculated (Bhalla and Karim, 1989; Badnell, 1990), and the present and previously (Schulz et al., 1988) measured RTE cross sections for the F^{6+} + H_2 system as functions of projectile energy. It is clear that the present measured RTE cross section values are substantially larger (by about 70%) than those obtained at the Oak Ridge National Laboratory (ORNL). Hence, taking into consideration the systematic experimental

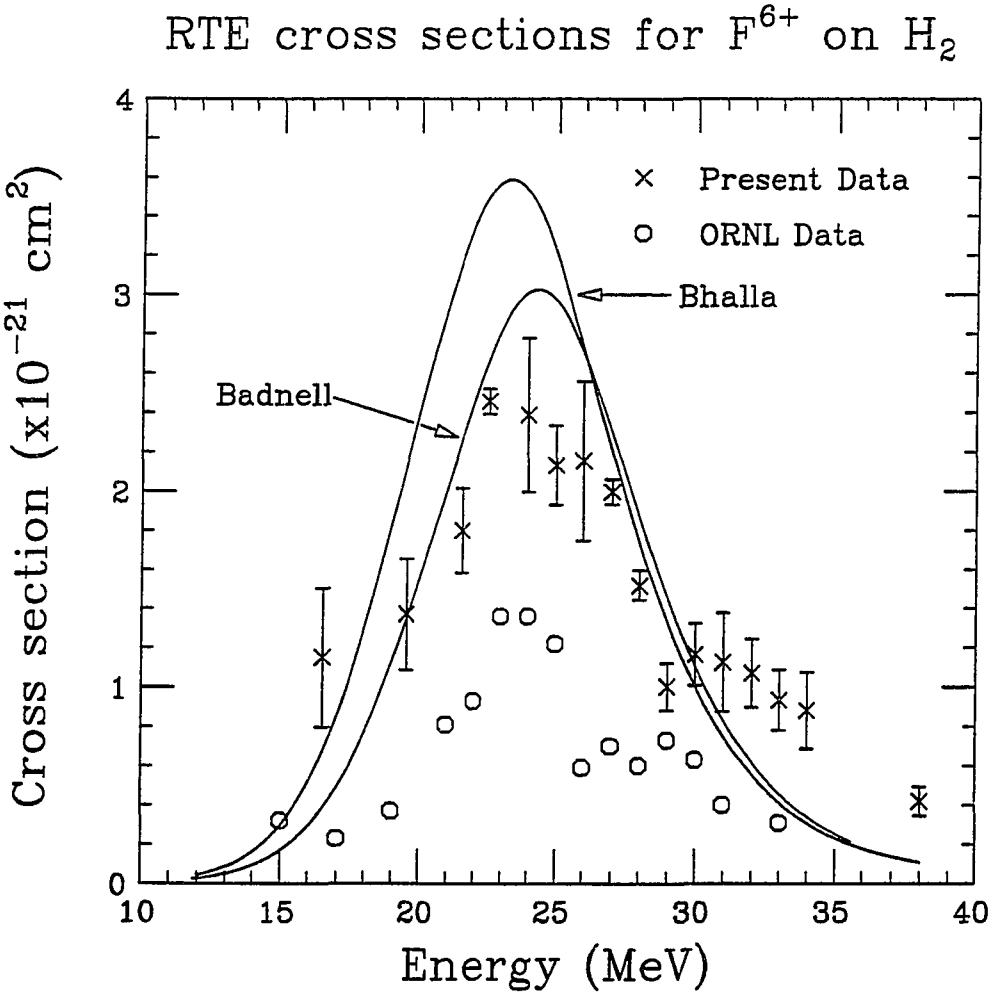

Figure 16. Calculated and Experimental RTE Cross Sections for F^{6+} + H_2 as a Function of Projectile Energy.

uncertainties which are estimated to be about 30%, we see that the present data are in reasonable agreement with the theory. Also, comparing the present data with the measurements made at ORNL we observe that the energy dependence of the contribution to the cross section on the high energy side of the resonant maximum appears somewhat different.

In Figure 17 the measured cross sections for capture and simultaneous emission of an x ray versus projectile energy for F^{6+} + He, F^{8+} + He, and F^{9+} + He are presented. For the F^{8+} + He and F^{9+} + He systems no resonant behavior is observed and the data have the shape of the capture probability curve as seen for the F^{8+} + H_2 system. In the case of F^{6+} + He only three data points were measured since extremely long running times were required in order to get data of sufficient statistical quality.

Figure 18 shows the measured cross sections for total K x-ray production versus projectile energy for the F^{6+} + He, F^{8+} + He, and F^{9+} + He systems. For F^{6+} + He a maximum in the excitation cross section should occur near 36 MeV. But these data do not at all resemble the characteristics of an excitation cross section. The reason for this is unclear except that metastable states in F^{6+} may give rise to K x-ray emission via a capture event, but then this should also be the case for the F^{6+} + H_2 data.

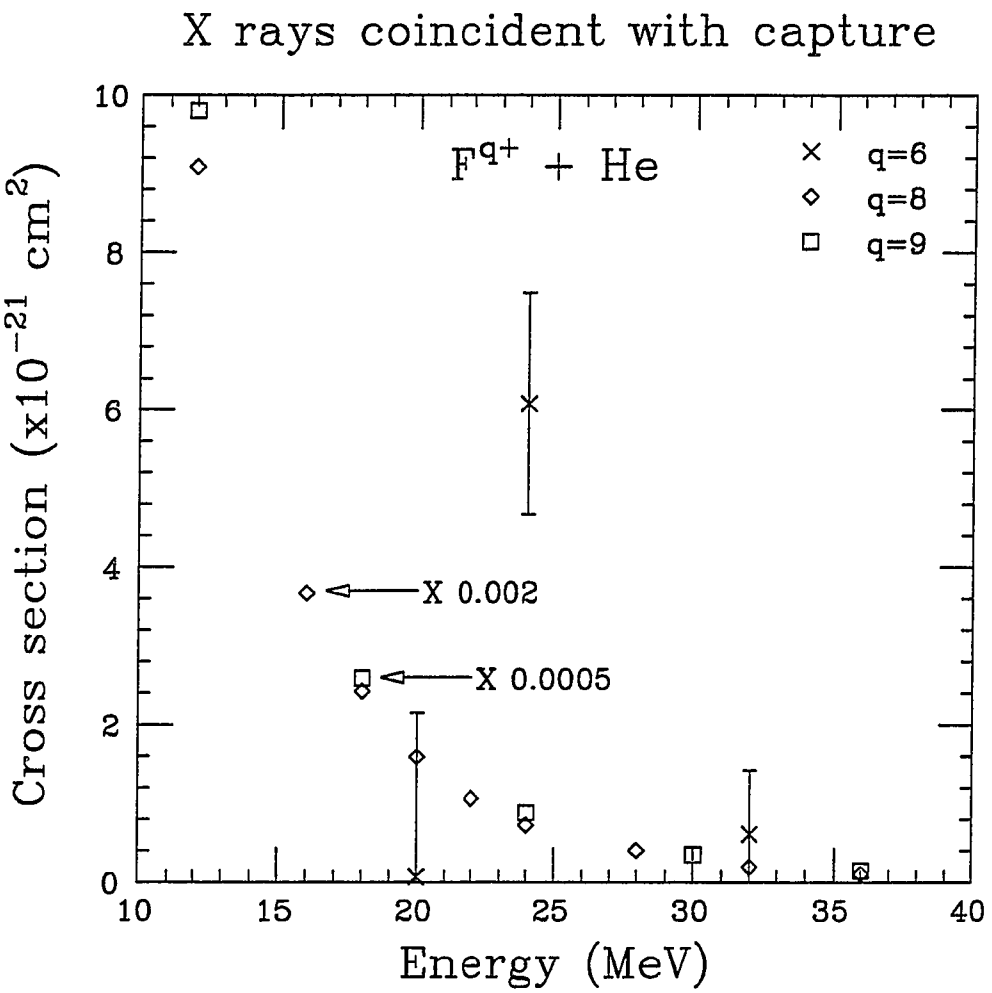

Figure 17. Measured Cross Sections for Capture and Simultaneous Emission of a K x-ray Versus Projectile Energy for F^{6+} + He, F^{8+} + He, and F^{9+} + He.

Table 4

Cross Sections for Single Electron Capture Coincident With K x-ray Emission for F^{q+} + He

q	Energy (Mev)	σ^{x}_{q-1} ($x10^{-19}cm^2$)	Uncertainty ($x10^{-19}cm^2$)
6	20	0.00067	0.021
6	24	0.061	0.023
6	32	0.0061	0.008
8	9.5	99.7	30.1
8	12	45.4	13.7
8	16	18.4	5.53
8	18	12.1	3.66
8	20	7.95	2.40
8	22	5.31	1.60
8	24	5.63	1.09
8	28	2.02	0.62
8	32	0.96	0.29
8	36	0.53	0.16
9	12	196.0	59.1
9	18	51.8	15.6
9	24	17.6	5.31
9	30	6.98	2.10
9	36	2.88	0.87

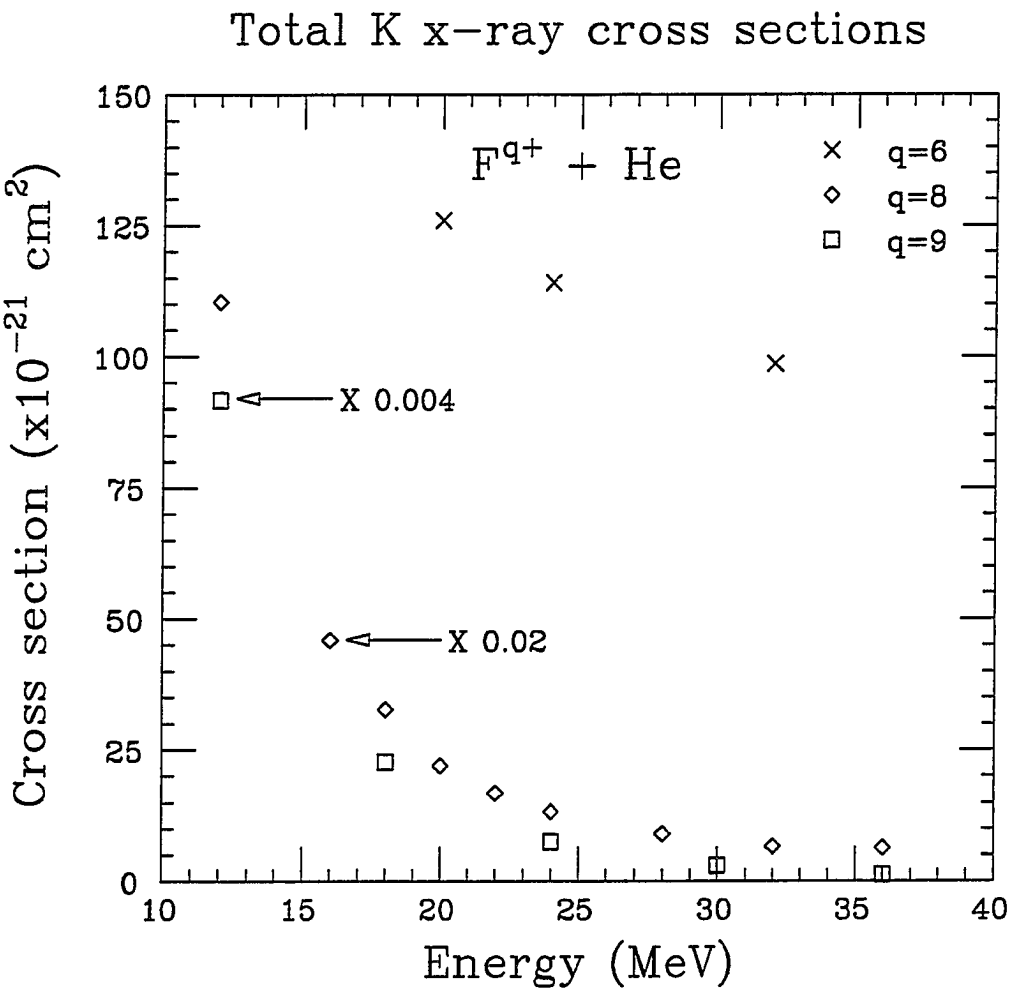

Figure 18. Measured Cross Sections for Total K x-ray Production Versus Projectile Energy for F^{6+} + He, F^{8+} + He, and F^{9+} + He.

Table 5

Cross Sections for Total K x-ray Production for F^{q+} + He

q	Energy(Mev)	σ_x(x10^{-19}cm^2)	Uncertainty(x10^{-19}cm^2)
6	20	1.26	0.38
6	24	1.14	0.34
6	32	0.98	0.30
8	9.5	130.0	39.0
8	12	55.2	16.6
8	16	22.9	6.89
8	18	16.3	4.91
8	20	11.0	3.30
8	22	8.41	2.53
8	24	6.64	2.00
8	28	4.52	1.36
8	32	3.31	0.99
8	36	3.17	0.95
9	12	229.0	68.9
9	18	56.6	17.0
9	24	18.8	5.65
9	30	7.4	2.23
9	36	2.9	0.88

At low energies, the F^{8+} and F^{9+} data exhibit the characteristics of electron capture. For F^{8+}, excitation can also give rise to a K x ray with a maximum probability near 38 MeV. Again, these F^{8+} cross sections are significantly larger than the F^{6+} cross sections indicating that a combination of both electron capture and electron excitation are responsible for the larger contribution of x rays as in the case of the $F^{8+} + H_2$ data.

In Figure 19 the coincidence and total x-ray production cross sections for both F^{9+} + He and $F^{9+} + H_2$ systems are presented. Referring to this figure and taking into consideration the systematic errors involved (i.e., errors giving rise to the uncertainties in δ) one sees that for each system the coincidence and x-ray cross sections are identical, something that is expected of course since capture is the only process giving rise to x-ray emission for bare projectiles. The same figure also indicates that the probability for electron capture (to n $\geq$ 2 levels) by a bare F ion is larger by about a factor of 14 when He rather than molecular hydrogen is used as the target. This result is consistent with previous related measurements for both O^{8+} + He and $O^{8+} + H_2$ (Boman et al., 1989).

Figure 20 presents the coincidence and total K x-ray production cross sections for F^{8+} + He and $F^{8+} + H_2$. First

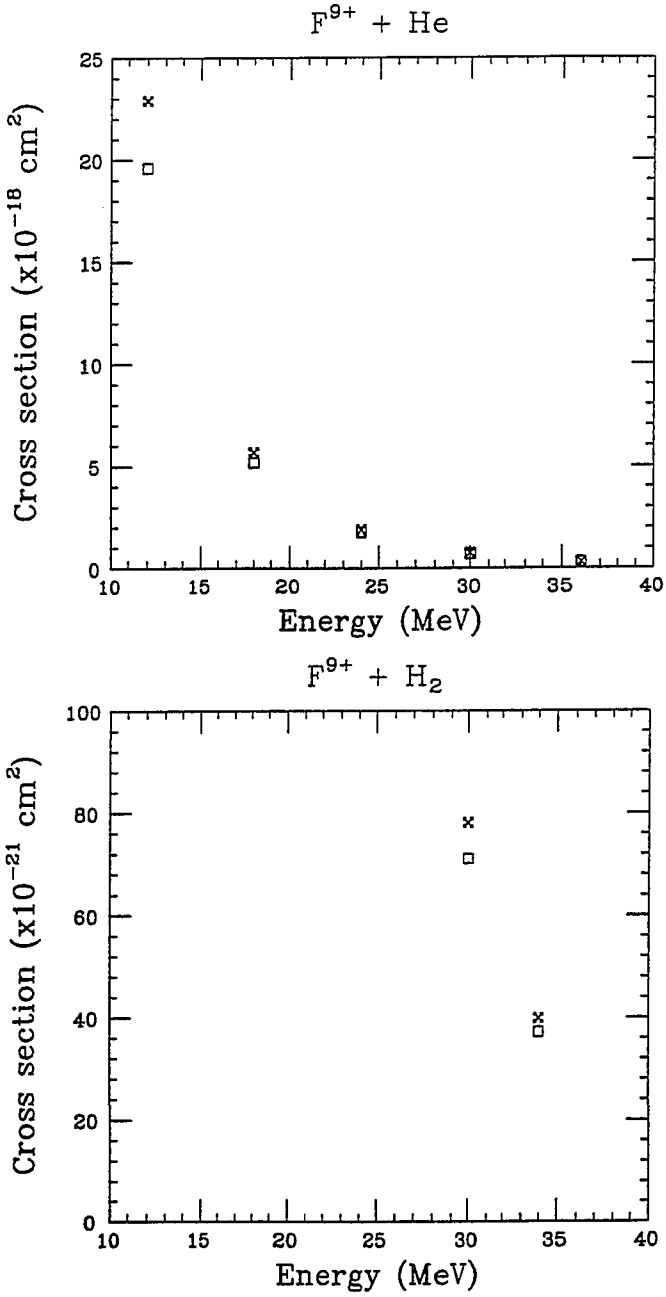

Figure 19. Coincidence (Squares) and Total x-ray Production (Stars) Cross Sections Versus Projectile Energy for the F^{9+} + He and F^{9+} + H_2 Systems.

of all, it can be seen that for each system the coincidence and x-ray cross sections are not identical as for the F^{9+} data. For both F^{8+} + He and F^{8+} + H_2, the total K x-ray production cross sections are significantly larger than the coincidence cross sections which indicates that capture is not the only process involved here but rather that excitation plays a considerable role in K x-ray emission. It can also be seen that for both systems the percent difference between coincidence and x-ray cross sections increases as the projectile energy increases. This implies that at low energies electron capture is the dominant process giving rise to K x rays while the excitation mechanism is responsible for K x-ray production at high energies. This is more evident from the F^{8+} + He data since the energy region studied for this system includes both low and high energies. The F^{8+} + H_2 data were taken at relatively high energies (i.e., 20 MeV to 34 MeV) and the total K x-ray cross sections are larger than the coincidence cross sections by at least a factor of 2.5 indicating that, for this high energy region, most of the K x rays emitted from a F^{8+} ion are due to the excitation mechanism. This result, together with the previous observation that the x-ray cross sections for F^{8+} are much larger than those for F^{6+}, imply that electron excitation is a process that takes place more frequently when F^{8+} rather

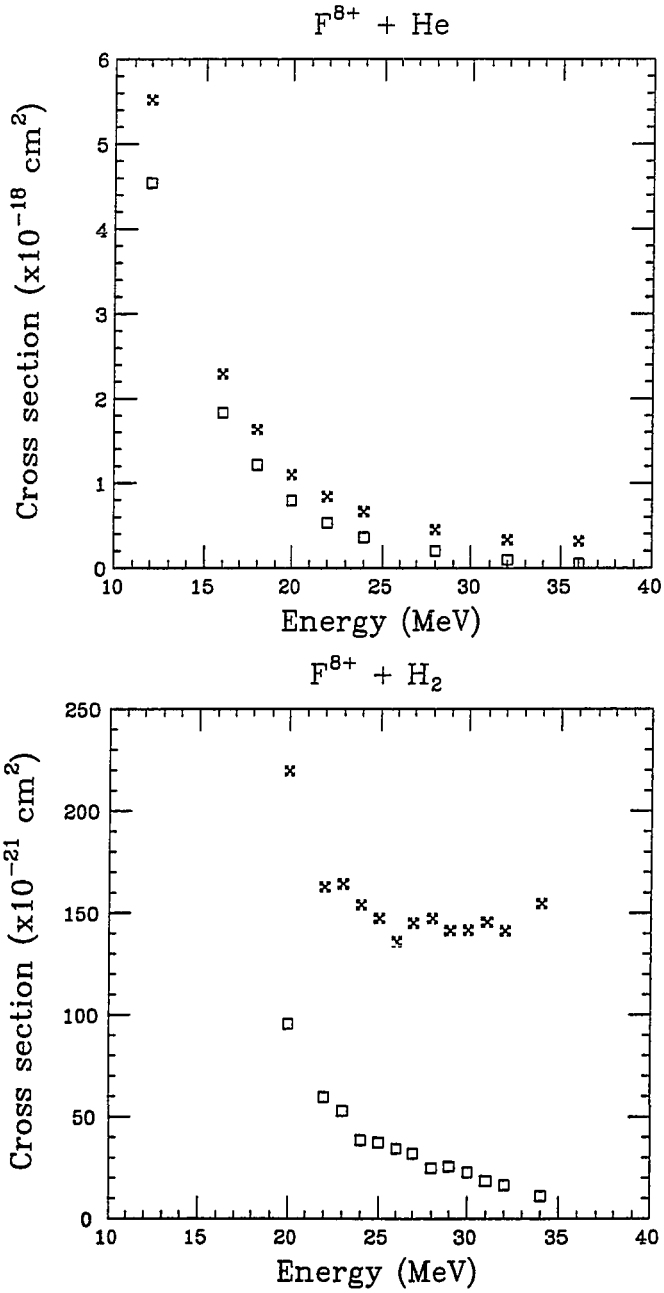

Figure 20. Coincidence (Squares) and Total x-ray Production (Stars) Cross Sections Versus Projectile Energy for the F^{8+} + He and F^{8+} + H_2 Systems.

than F^{6+} is used as the projectile. The F^{8+} + He data are also consistent with this observation.

The same figure also indicates that the percent difference between coincidence and x-ray cross sections for the F^{8+} + H_2 system is larger than that for the F^{8+} + He system and thus once again it is evident that the probability of an electron capture (to the $n \geq 2$ levels) by the projectile ion is larger when He rather than H_2 is used as the target.

Finally, Figures 21 and 22 show reduced plots of the total single-electron capture cross sections for F^{q+} ions with q = 6, 8, 9 incident on H_2 and He targets. The reduced electron-capture cross sections and the reduced projectile energies are given respectively by (Schlachter et al., 1987).

$$\tilde{\sigma} = \sigma\left[\frac{(Z^{1.8})}{(q^{0.7})}\right] \qquad (4.19)$$

$$\tilde{E} = \frac{E}{(Z^{1.25}.q^{0.5})} \qquad (4.20)$$

where σ is the measured single-electron capture cross section, Z is the atomic number of the target, q is the charge state of the projectile ion, and E is the projectile energy (keV/u).

It should be noted that the electron-capture cross

sections in H_2 were treated here by dividing the measured molecular cross sections by 2 and then using Z = 1. An empirical prediction (Schlachter et al., 1987) for the measured cross sections given by:

$$\tilde{\sigma} = 3.52x10^{-9}[1-\exp(-0.083\tilde{E}^{1.33})]\ x \\ x\ [1-\exp(-7.5\ x\ 10^{-6}\tilde{E}^{2.85})]/\tilde{E}^{4.18} \qquad (4.21)$$

is also shown in Figures 21 and 22.

Referring to Figures 21 and 22, we see that the electron-capture measurements are in reasonable agreement with the empirical curve to the cross sections except that the $F^{6+} + H_2$ data appear to deviate somewhat from the fit at high energies.

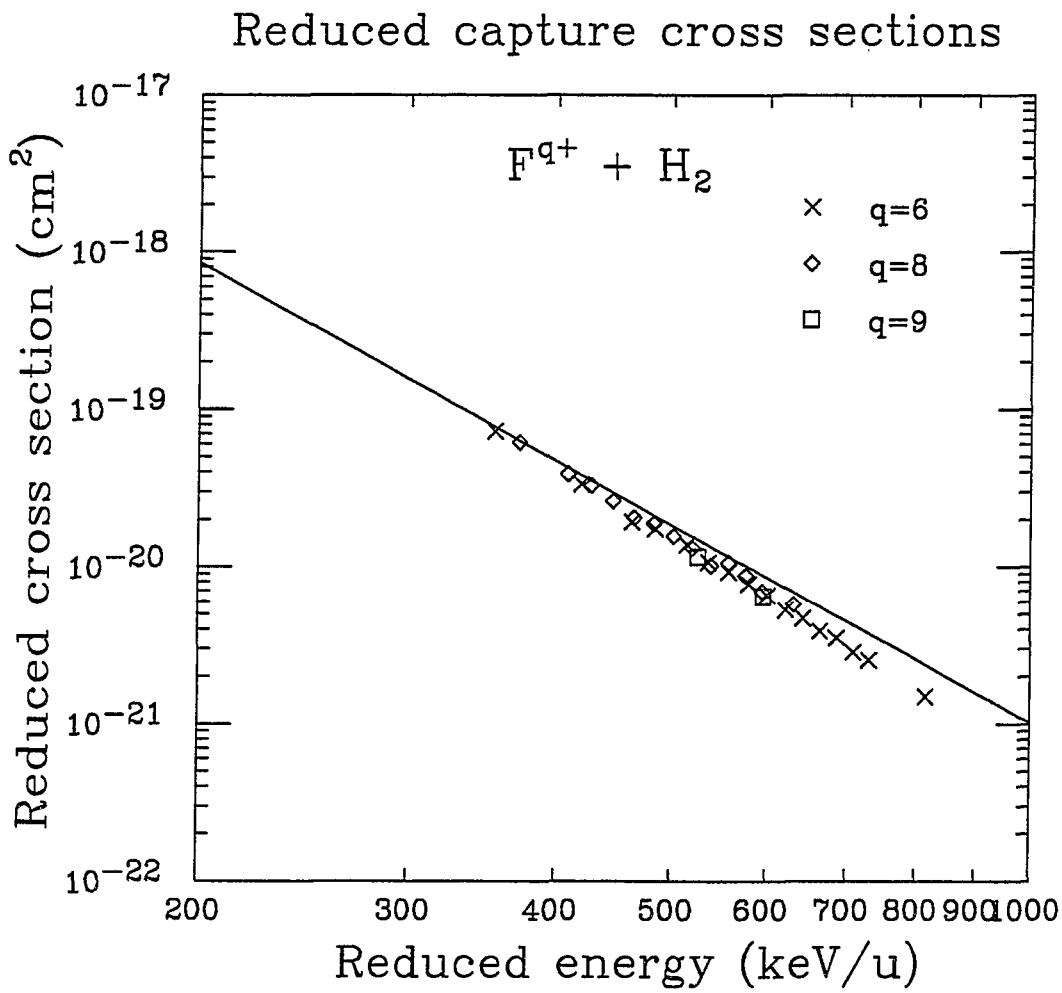

Figure 21. Reduced Plot of the Single-Electron Capture Cross Sections for F^{q+} Ions With q=6,8,9 Incident on H_2. The Solid Curve is the Empirical Curve of Schlachter et al., 1987.

Table 6

Single Electron-Capture Cross Sections for $F^{q+} + H_2$

q	Energy(Mev)	σ_{q-1}(x10^{-20}cm^2)	Uncertainty(x10^{-20}cm^2)
6	16.5	50.4	10.1
6	19.5	23.3	4.66
6	21.6	13.4	2.68
6	22.6	12.2	2.44
6	24	9.66	1.97
6	25	7.47	1.56
6	26	6.46	1.29
6	27	5.41	1.08
6	28	4.58	0.92
6	29	3.72	0.74
6	30	3.28	0.66
6	31	2.71	0.54
6	32	2.45	0.49
6	33	1.99	0.40
6	34	1.77	0.35
6	38	1.03	0.21
8	20	52.5	10.5
8	22	33.1	6.62
8	23	28.1	5.61
8	24	22.3	4.46
8	25	17.5	3.49
8	26	16.1	3.21
8	27	13.3	2.66
8	28	11.2	2.24
8	29	8.66	1.73
8	30	9.03	1.81
8	31	7.46	1.49
8	32	5.92	1.18
8	34	4.91	0.98
9	30	10.7	2.15
9	34	5.96	1.19

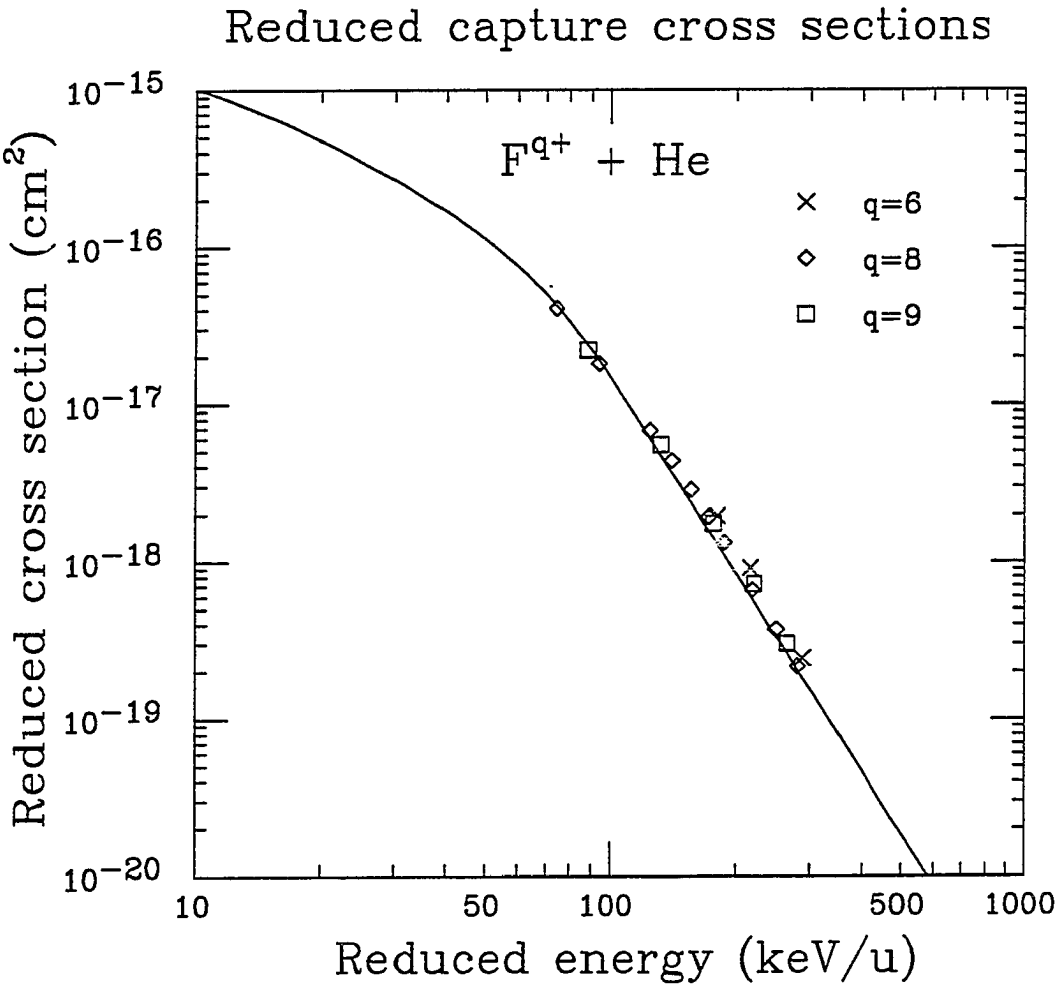

Figure 22. Reduced Plot of the Single-Electron Capture Cross Sections for F^{q+} Ions With q=6,8,9 Incident on He. The Solid Curve is the Empirical Curve of Schlachter et al., 1987.

Table 7

Single Electron-Capture Cross Sections for F^{q+} + He

q	Energy(Mev)	σ_{q-1}($x10^{-18}cm^2$)	Uncertainty($x10^{-18}cm^2$)
6	20	1.96	0.39
6	24	0.92	0.18
6	32	0.24	0.49
8	9.5	50.0	10.0
8	12	22.4	4.49
8	16	8.39	1.68
8	18	5.39	1.08
8	20	3.54	0.71
8	22	2.37	0.47
8	24	1.63	0.33
8	28	0.82	0.16
8	32	0.46	0.09
8	36	0.27	0.05
9	12	29.8	5.95
9	18	7.39	1.48
9	24	2.35	0.47
9	30	0.97	0.19
9	36	0.41	0.08

CHAPTER V

CONCLUSION

The data obtained in the present experiment exhibit resonant behavior in the σ^{x}_{q-1} cross section very near to the energies predicted by RTE theory for the case of F^{6+} projectile ions incident on H_2. It is clear that the measured RTE cross section values are substantially larger (by about 70%) than those obtained at the Oak Ridge National Laboratory and the present values are in reasonable agreement with theory. The competing process of NTE does not appreciably interfere with the observation of the resonant process since it is dominant at projectile energies lower than those for which RTE occurs.

The σ^{x}_{q-1} data also show a contribution greater than that predicted by theory on the high energy side of the resonant maximum but the energy dependence in this region appears somewhat different from that observed in the ORNL data. At present, the origin of this high-energy contribution is not clear and further investigation is necessary to understand the mechanism responsible.

For F^{6+} + He, the data were insufficient to make any quantitative assessment of RTE. For F^{8+} + H_2 and F^{8+} + He, no

resonant behavior was observed and the cross sections for capture and simultaneous emission of a K x ray decrease as the projectile energy increases, a feature that is characteristic of the capture probability function. This behavior was expected since an F^{8+} ion has only one electron in the K shell, and therefore, except for capture to the K shell and the formation of metastable states, each projectile with a charge reduced by one unit (i.e., a capture event) should lead to a K x-ray event. Thus, for these systems σ^{x}_{q-1} is dominated by charge transfer to $n \geq 2$.

In the case of $F^{6+} + H_2$, the total K x-ray emission cross section curve has the shape characteristic of an excitation cross section as expected since, for a F^{6+} projectile, K-shell excitation gives rise to x-ray emission. The maximum in this cross section should occur near 36 MeV since at that energy $V_{ion}=V_{electron.}$ For F^{6+} + He, a maximum in the excitation cross section should also occur near 36 MeV but these data do not resemble the characteristics of an excitation cross section. The reason for this is unclear except that metastable states in F^{6+} may give rise to K x-ray emission via a capture event. For the $F^{8+} + H_2$, $F^{9+} + H_2$, F^{8+} + He, and F^{9+} + He data, the total K x-ray emission cross section values generally decrease with increasing energy. For F^{8+}, excitation can also give rise to a K x-ray with a maximum probability near 38 MeV. These

F^{8+} cross sections are larger than the F^{6+} cross sections, even at relatively high energies, indicating that these x rays are the result of the combination of both electron capture and electron excitation with excitation occurring more frequently than it does in the case of F^{6+}. The F^{9+} + He and F^{9+} + H_2 data also indicate that the probability for electron capture (to $n \geq 2$ levels) by a bare F ion is larger by about a factor of 14 when He rather than molecular hydrogen is used as the target. For both the F^{8+} + H_2 and F^{8+} + He systems, the total K x-ray production cross sections are larger than the coincidence cross sections indicating that capture is not the only process involved but rather that the excitation mechanism participates considerably in the x-ray production process. It can also be seen that for both systems the percent difference between coincidence and x-ray cross sections increases as the projectile energy increases. This indicates that at low energies electron capture is the dominant process giving rise to K x rays while the excitation mechanism is responsible for K x-ray emission at high energies. The F^{8+} + H_2 data which were taken at the highest energies show that the total K x-ray cross sections are larger than the coincidence cross sections by at least a factor of 2.5 indicating that most of the x rays emitted from a F^{8+} ion are due to the excitation mechanism. This

observation together with the result that the x-ray cross sections for F^{8+} are much larger than those for F^{6+} imply that electron excitation is more probable when F^{8+} rather than F^{6+} is used as the projectile. This interesting result is also justified by the F^{8+} + He data. Another observation is that the percent difference between coincidence and x-ray cross sections for the F^{8+} + H_2 system is larger than that for the F^{8+} + He system and thus once again it is evident that the probability for electron capture (to $n \geq 2$ levels) by the projectile ion is larger when He rather than H_2 is used as the target.

Finally, the reduced plots of the total single-electron capture cross sections for F^{q+} ions with q = 6,8,9 incident on H_2 and He show that the measurements are in reasonable agreement with an empirical fit to the cross sections except that the F^{6+} + H_2 data deviate somewhat from the fit at the highest energies.

BIBLIOGRAPHY

Badnell, N.R. (1990). private communication.

Bernstein, E.M. (1990). private communication.

Bernstein, E.M. (1991). private communication.

Bhalla, C.P., and Karim, K.R. (1989). Resonant transfer andexctation in collisions of Li-like F^{6+} and Ca^{17+} with light targets. Physical Review, A39, 6060-6063.

Bhatia, A.K., and Temkin, A. (1977). A distorted-wave methodology for electron-ion impact excitation: Calculation for two-electron ions. Journal of Physics, B10, 2893-2912.

Biggs, F., Mendelson, L.B., and Mann, J.B. (1975). Hartree-Fock Compton profiles for the elements. Atomic Data and Nuclear Data Tables, 16, 201-309.

Boman, S.A., Bernstein, E.M., and Tanis, J.A. (1989). Single-electron capture and loss cross sections versus target Z for 1 Mev/u oxygen ions incident on gases. Physical Review, A39, 4423-4427.

Brandt, D. (1983). Resonant transfer and excitation in ion-atom collisions. Physical Review, A27, 1314-1318.

Clark, M.W. (1989). private communication.

Feagin, J.M., Briggs, J.S., and Reeves, T.M. (1984). Simultaneous charge transfer and excitation. Journal of Physics, B17, 1057 - 1068.

Hahn, Y. (1985). private communication to Tanis, J.A., and Bernstein, E.M.

Hahn, Y., Ramadan, H., (1989). Uncorrelated transfer excitation collisions at high energies. Physical Review, A40, 6206 - 6209.

Hasted, J.B. (1972). Physics of Atomic Collisions (2nd ed.) New York: Elsevier.

Khandelwal, G.S., Choi, B.H., and Merzbacher, E. (1969). Ionization by heavy particles. Atomic Data, Vol 1, 103-120.

McLaughlin, D.J., and Hahn, Y. (1982). Dielectronic recombination cross sections for Si^{11+} and S^{13+}. Physics Letters, 88A, 394 - 397.

Nasser, I., and Hahn, Y. (1983). Dielectronic recombination rates for heliumlike ions. Journal of Quantum Spectroscopy and Radiation Transfer, 29, 1-8.

Pepmiller, P.L. (1983). Formation of doubly excited two electron ions during F^{8+} + He, Ne, or Ar collisions. Doctoral dissertation, Kansas State University, Manhattan, KS.

Pepmiller, P.L., Richard, P., Newcomb, J., Hall, J., and Dillingham, T.R. (1985). Formation of doubly excited two-electron ions during F^{8+} + He, F^{8+} + Ne, F^{8+} + Ar collisions. Physical Review, A31, 734.

Reeves, T.M., Feagin, J.M., and Merzbacher, E., Abstracts of Contributed Papers, 14th International Conference on the Physics of Electronic and Atomic Collisions, Palo Alto, California (1985), 392.

Roszman, L.J. (1979). Dielectronic recombination rate of Mo XXXIII. Physical Review, A20, 673 - 676.

Schlachter, A.S., Stearns, J.W., Berkner, K.H., Stockli, M.P., Graham, W.G., Bernstein, E.M., Clark, M.W., and Tanis, J.A., Abstracts of Contributed Papers, Proceedings of the Fifteenth International Conference of the Physics of Electronic and Atomic Collisions, Brighton, United Kingdom, 1987, edited by Gedes, J., Gilbody, H.B., Kingston, A.E., Latimer, C.J., and Walters, H.J.R. (Queens University, Belfast, 1987), 505.

Schulz, M., Giese, J.P., Swenson, J.K., Datz, S., Dittner, P.F., Krause, H.F., Schone, H., Vane, C.R., Benhenni, M., and Shafroth, S.M. (1989). Electron-Electron Interaction in Transfer and Excitation in F^{8+} -> H_2 Collisions. Physical Review Letters, 62, 1738-1741.

Schulz, M., Schuch, R., Datz, S., Justiniano, E.L.B., Miller, P.D., and Schone, H. (1988). Resonant transfer and excitation in Li-like F colliding with H_2.

Physical Review, A38, 5454-5457.

Seaton, M.J., and Storey, P.J. (1976). Dielectronic recombination. In P.G. Burke and B.L. Moiseiwitsch (Eds.), Atomic processes and applications (pp. 133-197). New York: North Holland Publishing.

Swenson, J.K., Yamazaki, Y., Miller, P.D., Krause, H.F., Dittner, P.F., Pepmiller, P.L., Datz, S., and Stolterfoht, N. (1986). Observation of Resonant Transfer and Excitation to Specific LS-Coupled states in O_{5+} + He Collisions by High-Resolution, 0° Auger-Electron Spectroscopy. Physical Review Letters, 57, 3042-3045.

Tanis, J.A., Bernstein, E.M., Clark, M.W., Graham, W.G., McFarland, R.H., Morgan, T.J., Johnson, B.M., Jones K.W., and Meron, M. (1985). Evidence for uncorrelated electron capture and K-shell excitation in S^{13+} + He collisions. Physical Review, A31, 4040-4042.

Tanis, J.A., Bernstein, E.M., Graham, W.G., Stockli, M.P., Clark, M., McFarland, R.H., Morgan, T.J., Berkner, K.H., Schlachter, A.S., and Stearns, J.W. (1984). Resonant electron transfer and excitation in 2-, 3-, and 4-electron $_{20}Ca^{q+}$ and $_{23}V^{q+}$ ions colliding with helium. Physical Review Letters, 53, 2551-2554.

Tanis, J.A., Shafroth, S.M., Willis, J.E., Clark, M., Swenson, J.K., Strait, E.M., and Mowat, J.R. (1981). Simultaneous electron capture and excitation in S + Ar Collisions. Physical Review Letters, 47, 828-831.

Tawara, H., Terasawa, M., Richard, P., Gray, T.J., Pepmiller, P., Hall, J., and Newcomb, J. (1979). Role of excitation in K-shell vacancy production for F^{6+} + He Collisions. Physical Review, A20, 2340 - 2345.